arXiv:hep-ph/9904472v2 28 Jul 1999

BI-TP 99/10
PSI-PR-99-12
hep-ph/9904472

Predictions for all processes $e^+e^- \to 4$ fermions $+ \gamma$

A. Denner[1], S. Dittmaier[2], M. Roth[1,3] and D. Wackeroth[1]

[1] *Paul-Scherrer-Institut, Würenlingen und Villigen*
CH–5232 Villigen PSI, Switzerland

[2] *Theoretische Physik, Universität Bielefeld*
D-33615 Bielefeld, Germany

[3] *Institut für Theoretische Physik, ETH-Hönggerberg*
CH–8093 Zürich, Switzerland

Abstract:

The complete matrix elements for $e^+e^- \to 4f$ and $e^+e^- \to 4f\gamma$ are calculated in the Electroweak Standard Model for polarized massless fermions. The matrix elements for all final states are reduced to a few compact generic functions. Monte Carlo generators for $e^+e^- \to 4f$ and $e^+e^- \to 4f\gamma$ are constructed. We compare different treatments of the finite widths of the electroweak gauge bosons; in particular, we include a scheme with a complex gauge-boson mass that obeys all Ward identities. The detailed discussion of numerical results comprises integrated cross sections as well as photon-energy distributions for all different final states.

April 1999

1 Introduction

When exceeding the W-pair production threshold, the LEP collider started a new era in the verification of the Electroweak Standard Model (SM): the study of the properties of the W boson and of its interactions. While the most important process at LEP2 in this respect is certainly $\mathrm{e^+e^-} \to \mathrm{W^+W^-} \to 4f$, many other reactions have now become accessible. Besides the 4-fermion-production processes, including single W-boson production, single Z-boson production, or Z-boson-pair production, LEP2 and especially a future linear collider allow us to investigate another class of processes, namely $\mathrm{e^+e^-} \to 4f\gamma$.

The physical interest in the processes $\mathrm{e^+e^-} \to 4f\gamma$ is twofold. First of all, they are an important building block for the radiative corrections to $\mathrm{e^+e^-} \to 4f$, and their effect must be taken into account in order to get precise predictions for the observables that are used for the measurement of the W-boson mass and the triple-gauge-boson couplings. On the other hand, those processes themselves involve interesting physics. They include, in particular, triple-gauge-boson-production processes such as $\mathrm{W^+W^-}\gamma$, $\mathrm{ZZ}\gamma$, or $\mathrm{Z}\gamma\gamma$ production and can therefore be used to obtain information on the quartic gauge-boson couplings $\gamma\gamma WW$, γZWW, and $\gamma\gamma ZZ$. While only a few events of this kind are expected at LEP2, these studies can be performed in more detail at future linear $\mathrm{e^+e^-}$ colliders [1].

Important contributions to $\mathrm{e^+e^-} \to 4f$ and $\mathrm{e^+e^-} \to 4f\gamma$ arise from subprocesses with two resonant gauge bosons. These subprocesses do not only contain interesting physics, such as the quartic gauge-boson self-interactions, but also dominate the cross sections in those regions of phase space where the invariant masses of certain combinations of final-state particles are close to the mass of the corresponding nearly resonant gauge bosons. Therefore, it is sometimes a reasonable approach to consider only the resonant contributions. In the most naive approximation, the produced gauge bosons are treated as stable particles. Most of the existing calculations for triple-gauge-boson production have been performed in this way, such as many calculations for $\mathrm{e^+e^-} \to \mathrm{W^+W^-}\gamma$ [2].

In an improved approach, the so-called pole expansion [3, 4], the resonances are treated exactly, i.e. the decay of the produced gauge bosons is taken into account, but the matrix elements are expanded about the poles of the resonances. Once the non-resonant diagrams have been left out, the expansion is in fact mandatory in order to retain gauge invariance. If only the leading terms in the expansion are kept, this approach is known as the pole approximation, or double-pole approximation in the presence of two resonances. The accuracy of the (double-)pole approximation is, at best, of the order of $\Gamma_\mathrm{V}/M_\mathrm{V}$, where M_V and Γ_V are the mass and the width of the relevant gauge bosons, and thus typically at the level of several per cent. Consequently, this approach is only reasonable if the experimental accuracy is correspondingly low. The error estimate of $\Gamma_\mathrm{V}/M_\mathrm{V}$ is too optimistic in situations in which scales of order Γ_V, or smaller, are involved. This is, in particular, the case in threshold regions or if photons with energies of the order of Γ_V are emitted from the resonant gauge bosons. On the other hand, the quality of the pole approximation can be improved by applying appropriate invariant-mass cuts.

Note that the double-pole approximation is particularly well-suited for the calculation of the radiative corrections to gauge-boson pair production, since the error resulting from the double-pole approximation is suppressed by an additional factor α/π in this case. In this approximation the corrections can be classified into factorizable and non-factorizable corrections [4, 5]. The virtual factorizable corrections can be composed of the known corrections to on-shell W-pair production [6] and on-shell W decay [7], and the non-factorizable corrections have recently been calculated [8]. In contrast to the virtual factorizable corrections, the real factorizable corrections cannot be simply taken over from the on-shell processes. In the case of real photon emission the definition of the double-pole approximation is non-trivial if the energy of the final-state photon is of the order of Γ_{V}, since the resonances before and after photon emission are not well separated in phase space. A possible double-pole approximation of the $\mathcal{O}(\alpha)$ corrections to four-lepton production has been discussed in Ref. [9].

In our calculation of $\mathrm{e}^+\mathrm{e}^- \to 4f\gamma$ we do not use the double-pole approximation since the full calculation is feasable with reasonable effort. Unlike the double-pole approximation, the full calculation is valid for arbitrary processes in the set $\mathrm{e}^+\mathrm{e}^- \to 4f\gamma$. Moreover, when using the exact results for the real corrections in an $\mathcal{O}(\alpha)$ calculation of 4 fermion-production processes, the reliability of possible approximations can be tested.

Some results for $\mathrm{e}^+\mathrm{e}^- \to 4f\gamma$ with an observable photon already exist in the literature. In Refs. [10, 11] the contributions to the matrix elements involving two resonant W bosons have been calculated and implemented into a Monte Carlo generator. This generator has been extended to include collinear bremsstrahlung [12] and used to discuss the effect of hard photons at LEP2 [13]. The complete cross section for the process $\mathrm{e}^+\mathrm{e}^- \to \mathrm{u}\,\bar{\mathrm{d}}\,\mathrm{e}^-\bar{\nu}_{\mathrm{e}}\gamma$ has been discussed in Ref. [14]. In Ref. [15], the complete matrix elements for the processes $\mathrm{e}^+\mathrm{e}^- \to 4f\gamma$ have been calculated using an iterative numerical algorithm without referring to Feynman diagrams. We are, however, interested in explicit analytical results on the amplitudes for various reasons. In particular, we want to have full control over the implementation of the finite width of the virtual vector bosons and to select single diagrams, such as the doubly-resonant ones. So far no results for $\mathrm{e}^+\mathrm{e}^- \to 4f\gamma$ with $\mathrm{e}^+\mathrm{e}^-$ pairs in the final state have been published.

In order to perform the calculation as efficient as possible we have reduced all processes to a small number of generic contributions. For $\mathrm{e}^+\mathrm{e}^- \to 4f$, the calculation is similar to the one in Ref. [16], and the generic contributions correspond to individual Feynman diagrams. In the case of $\mathrm{e}^+\mathrm{e}^- \to 4f\gamma$ we have combined groups of diagrams in such a way that the resulting generic contributions can be classified in the same way as those for $\mathrm{e}^+\mathrm{e}^- \to 4f$. As a consequence, the generic contributions are individually gauge-invariant with respect to the external photon. The number and the complexity of diagrams in the generic contributions for $\mathrm{e}^+\mathrm{e}^- \to 4f\gamma$ has been reduced by using a non-linear gauge-fixing condition for the W-boson field [17]. In this way, many cancellations between diagrams are avoided, without any further algebraic manipulations. Finally, for the helicity amplitudes corresponding to the generic contributions concise results have been obtained by using the Weyl–van der Waerden formalism (see Ref. [18] and references therein).

After the matrix elements have been calculated, the finite widths of the resonant particles have to be introduced. We have done this in different ways and compared the different treatments for $\mathrm{e}^+\mathrm{e}^- \to 4f$ and $\mathrm{e}^+\mathrm{e}^- \to 4f\gamma$. In particular, we have discussed a "complex-mass scheme", which preserves all Ward identities and is still rather simple to apply.

The matrix elements to $\mathrm{e}^+\mathrm{e}^- \to 4f$ and $\mathrm{e}^+\mathrm{e}^- \to 4f\gamma$ exhibit a complex peaking behaviour owing to propagators of massless particles and Breit–Wigner resonances, so that the integration over the 8- and 11-dimensional phase spaces, respectively, is not straightforward. In order to obtain numerically stable results, we adopt the multi-channel integration method [16, 19] and reduce the Monte Carlo error by the adaptive weight optimization procedure described in Ref. [20]. In the multi-channel approach, we define a suitable mapping of random numbers into phase space variables for each arising propagator structure. These variables are generated according to distributions that approximate this specific peaking behavior of the integrand. For $\mathrm{e}^+\mathrm{e}^- \to 4f$ and $\mathrm{e}^+\mathrm{e}^- \to 4f\gamma$ we identify up to 128 and 928 channels, respectively, which necessitates an efficient and generic procedure for the phase-space generation. We wrote two independent Monte Carlo programs following the general strategy outlined above. They differ in the realization of a generic procedure for the construction of the phase-space generators.

The paper is organized as follows: in Section 2 we describe the calculation of the helicity amplitudes for $\mathrm{e}^+\mathrm{e}^- \to 4f$ and $\mathrm{e}^+\mathrm{e}^- \to 4f\gamma$ and list the complete results. The Monte Carlo programs are described in Section 3. In Section 4 the numerical results are discussed, and Section 5 contains a summary and an outlook.

2 Analytical results

2.1 Notation and conventions

We consider reactions of the types

$$\mathrm{e}^+(p_+,\sigma_+) + \mathrm{e}^-(p_-,\sigma_-) \to f_1(k_1,\sigma_1) + \bar{f}_2(k_2,\sigma_2) + f_3(k_3,\sigma_3) + \bar{f}_4(k_4,\sigma_4), \tag{2.1}$$
$$\mathrm{e}^+(p_+,\sigma_+) + \mathrm{e}^-(p_-,\sigma_-) \to f_1(k_1,\sigma_1) + \bar{f}_2(k_2,\sigma_2) + f_3(k_3,\sigma_3) + \bar{f}_4(k_4,\sigma_4) + \gamma(k_5,\lambda). \tag{2.2}$$

The arguments label the momenta $p_\pm$, k_i and helicities $\sigma_i = \pm 1/2$, $\lambda = \pm 1$ of the corresponding particles. We often use only the signs to denote the helicities. The fermion masses are neglected everywhere.

For the Feynman rules we use the conventions of Ref. [21]. In particular, all fields and momenta are incoming. It is convenient to use a non-linear gauge-fixing term [17] of the form

$$\begin{aligned}\mathcal{L}_{\mathrm{fix}} = {} & -\left|\partial^\mu W^+_\mu + \mathrm{i}e(A^\mu - \frac{c_{\mathrm{w}}}{s_{\mathrm{w}}} Z^\mu) W^+_\mu - \mathrm{i} M_{\mathrm{W}} \phi^+\right|^2 \\ & - \frac{1}{2}(\partial^\mu Z_\mu - M_{\mathrm{Z}}\chi)^2 - \frac{1}{2}(\partial^\mu A_\mu)^2 ,\end{aligned} \tag{2.3}$$

where $\phi^\pm$ and χ are the would-be Goldstone bosons of the $W^\pm$ and Z fields, respectively. With this choice, the $\phi^\pm W^\mp A$ vertices vanish, and the bosonic couplings that are relevant for $\mathrm{e}^+\mathrm{e}^- \to 4f\gamma$ read

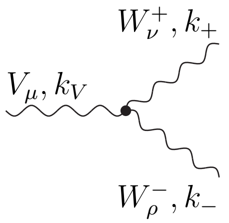

$$= -\mathrm{i}e g_{VWW} \left[g_{\nu\rho}(k_- - k_+)_\mu - 2 g_{\mu\nu} k_{V,\rho} + 2 g_{\mu\rho} k_{V,\nu} \right],$$

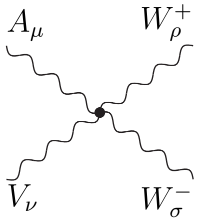

$$= -2\mathrm{i}e g_{VWW}\, g_{\mu\nu} g_{\rho\sigma}, \tag{2.4}$$

with $V = A, Z$, and the coupling factors

$$g_{AWW} = 1, \qquad g_{ZWW} = -\frac{c_{\mathrm{w}}}{s_{\mathrm{w}}}. \tag{2.5}$$

Note that the gauge-boson propagators have the same simple form as in the 't Hooft–Feynman gauge, i.e. they are proportional to the metric tensor $g_{\mu\nu}$. This gauge choice eliminates some diagrams and simplifies others owing to the simpler structure of the photon–gauge-boson couplings.

The vector-boson–fermion–fermion couplings have the usual form

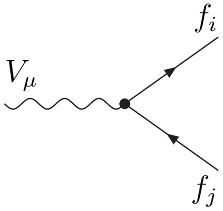

$$= \mathrm{i}e\gamma_\mu \sum_\sigma g^\sigma_{V\bar{f}_i f_j} \omega_\sigma, \tag{2.6}$$

where $\omega_\pm = (1 \pm \gamma_5)/2$. The corresponding coupling factors read

$$g^\sigma_{A\bar{f}_i f_i} = -Q_i, \qquad g^\sigma_{Z\bar{f}_i f_i} = -\frac{s_{\mathrm{w}}}{c_{\mathrm{w}}} Q_i + \frac{I^3_{\mathrm{w},i}}{c_{\mathrm{w}} s_{\mathrm{w}}} \delta_{\sigma-}, \qquad g^\sigma_{W\bar{f}_i f'_i} = \frac{1}{\sqrt{2} s_{\mathrm{w}}} \delta_{\sigma-}, \tag{2.7}$$

where Q_i and $I^3_{\mathrm{w},i} = \pm 1/2$ denote the relative charge and the weak isospin of the fermion f_i, respectively, and f'_i is the weak-isospin partner of f_i. The colour factor of a fermion f_i is denoted by $N^{\mathrm{c}}_{f_i}$, i.e. $N^{\mathrm{c}}_{\mathrm{lepton}} = 1$ and $N^{\mathrm{c}}_{\mathrm{quark}} = 3$.

2.2 Classification of final states for $\mathrm{e}^+\mathrm{e}^- \to 4f$

The final states for $\mathrm{e}^+\mathrm{e}^- \to 4f$ have already been classified in Refs. [16, 22, 23]. We introduce a classification that is very close to the one of Refs. [22, 23]. It is based on the production mechanism, i.e. whether the reactions proceed via charged-current (CC), or neutral-current (NC) interactions, or via both interaction types. The classification can be performed by considering the quantum numbers of the final-state fermion pairs. In the following, f and F denote different fermions ($f \neq F$) that are neither electrons nor electron neutrinos ($f, F \neq \mathrm{e}^-, \nu_{\mathrm{e}}$), and their weak-isospin partners are denoted by f' and F', respectively. We find the following 11 classes of processes (in parenthesis the corresponding classification of Ref. [23] is given):

(i) CC reactions:

  (a) $\mathrm{e}^+\mathrm{e}^- \to f\bar{f}'F\bar{F}'$, (*CC11* family),
  (b) $\mathrm{e}^+\mathrm{e}^- \to \nu_{\mathrm{e}}\mathrm{e}^+ f\bar{f}'$, (*CC20* family),
  (c) $\mathrm{e}^+\mathrm{e}^- \to f\bar{f}'\mathrm{e}^-\bar{\nu}_{\mathrm{e}}$, (*CC20* family),

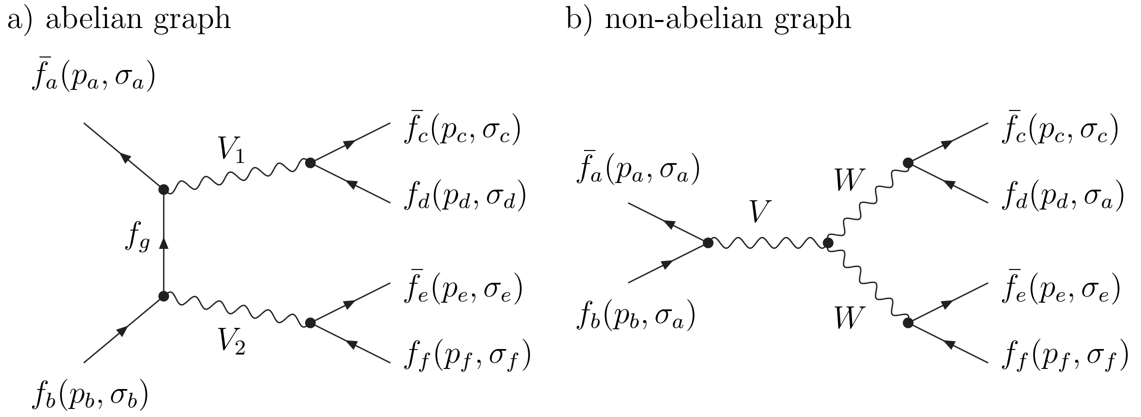

Figure 1: Generic diagrams for $e^+e^- \to 4f$

(ii) NC reactions:

  (a) $e^+e^- \to f\bar{f}F\bar{F}$, (*NC32* family),
  (b) $e^+e^- \to f\bar{f}f\bar{f}$, (*NC4·16* family),
  (c) $e^+e^- \to e^-e^+f\bar{f}$, (*NC48* family),
  (d) $e^+e^- \to e^-e^+e^-e^+$, (*NC4·36* family),

(iii) Mixed CC/NC reactions:

  (a) $e^+e^- \to f\bar{f}f'\bar{f}'$, (*mix43* family),
  (b) $e^+e^- \to \nu_e\bar{\nu}_e f\bar{f}$, (*NC21* family),
  (c) $e^+e^- \to \nu_e\bar{\nu}_e\nu_e\bar{\nu}_e$, (*NC4·9* family),
  (d) $e^+e^- \to \nu_e\bar{\nu}_e e^-e^+$, (*mix56* family).

The radiation of an additional photon does not change this classification.

2.3 Generic diagrams and amplitudes for $e^+e^- \to 4f$

In order to explain and to illustrate our generic approach we first list the results for $e^+e^- \to 4f$. All these processes can be composed from only two generic diagrams, the abelian and non-abelian diagrams shown in Figure 1. All external fermions $f_{a,\dots,f}$ are assumed to be incoming, and the momenta and helicities are denoted by $p_{a,\dots,f}$ and $\sigma_{a,\dots,f}$, respectively. The helicity amplitudes of these diagrams are calculated within the Weyl–van der Waerden (WvdW) formalism following the conventions of Ref. [18] (see also references therein).

2.3.1 Leptonic and semi-leptonic final states

We first treat purely leptonic and semi-leptonic final states. In this case, none of the gauge bosons in the generic graphs of Figure 1 can be a gluon, and the colour structure trivially leads to a global factor $N^{\mathrm{c}}_{f_1} N^{\mathrm{c}}_{f_3}$, which is equal to 1 or 3, after summing the squared amplitude over the colour degrees of freedom. The results for the generic amplitudes are

$$\begin{aligned}
&\mathcal{M}^{\sigma_a,\sigma_b,\sigma_c,\sigma_d,\sigma_e,\sigma_f}_{V_1V_2}(p_a,p_b,p_c,p_d,p_e,p_f) \\
&\quad = -4e^4 \delta_{\sigma_a,-\sigma_b}\delta_{\sigma_c,-\sigma_d}\delta_{\sigma_e,-\sigma_f}\, g^{\sigma_b}_{\mathrm{V}_1\bar{f}_a f_g} g^{\sigma_b}_{\mathrm{V}_2\bar{f}_g f_b} g^{\sigma_d}_{\mathrm{V}_1\bar{f}_c f_d} g^{\sigma_f}_{\mathrm{V}_2\bar{f}_e f_f} \\
&\qquad \times \frac{P_{\mathrm{V}_1}(p_c+p_d)P_{\mathrm{V}_2}(p_e+p_f)}{(p_b+p_e+p_f)^2}\, A_2^{\sigma_a,\sigma_c,\sigma_e}(p_a,p_b,p_c,p_d,p_e,p_f),
\end{aligned} \tag{2.8}$$

$$\begin{aligned}
&\mathcal{M}^{\sigma_a,\sigma_b,\sigma_c,\sigma_d,\sigma_e,\sigma_f}_{VWW}(p_a,p_b,p_c,p_d,p_e,p_f) \\
&\quad = -4e^4 \delta_{\sigma_a,-\sigma_b}\delta_{\sigma_c,+}\delta_{\sigma_d,-}\delta_{\sigma_e,+}\delta_{\sigma_f,-}\,(Q_c-Q_d) g_{VWW} g^{\sigma_b}_{V\bar{f}_a f_b} g^{-}_{W\bar{f}_c f_d} g^{-}_{W\bar{f}_e f_f} \\
&\qquad \times P_V(p_a+p_b)P_W(p_c+p_d)P_W(p_e+p_f)\, A_3^{\sigma_a}(p_a,p_b,p_c,p_d,p_e,p_f),
\end{aligned} \tag{2.9}$$

where the vector-boson propagators are abbreviated by

$$P_V(p) = \frac{1}{p^2 - M_{\mathrm{V}}^2}, \qquad V = A, Z, W, g, \qquad M_A = M_g = 0. \tag{2.10}$$

(The case of the gluon is included for later convenience.) The auxiliary functions $A_2^{\sigma_a,\sigma_c,\sigma_e}$ and $A_3^{\sigma_a}$ are expressed in terms of WvdW spinor products,

$$\begin{aligned}
A_2^{+++}(p_a,p_b,p_c,p_d,p_e,p_f) &= \langle p_a p_c\rangle \langle p_b p_f\rangle^* (\langle p_b p_d\rangle^* \langle p_b p_e\rangle + \langle p_d p_f\rangle^* \langle p_e p_f\rangle), \\
A_2^{++-}(p_a,p_b,p_c,p_d,p_e,p_f) &= A_2^{+++}(p_a,p_b,p_c,p_d,p_f,p_e), \\
A_2^{+-+}(p_a,p_b,p_c,p_d,p_e,p_f) &= A_2^{+++}(p_a,p_b,p_d,p_c,p_e,p_f), \\
A_2^{+--}(p_a,p_b,p_c,p_d,p_e,p_f) &= A_2^{+++}(p_a,p_b,p_d,p_c,p_f,p_e), \\
A_2^{-,\sigma_c,\sigma_d}(p_a,p_b,p_c,p_d,p_e,p_f) &= \left(A_2^{+,-\sigma_c,-\sigma_d}(p_a,p_b,p_c,p_d,p_e,p_f)\right)^*,
\end{aligned} \tag{2.11}$$

$$\begin{aligned}
A_3^{+}(p_a,p_b,p_c,p_d,p_e,p_f) = {}& \langle p_b p_d\rangle^* \langle p_b p_f\rangle^* \langle p_a p_b\rangle \langle p_c p_e\rangle + \langle p_b p_d\rangle^* \langle p_d p_f\rangle^* \langle p_a p_e\rangle \langle p_c p_d\rangle \\
& + \langle p_b p_f\rangle^* \langle p_d p_f\rangle^* \langle p_a p_c\rangle \langle p_e p_f\rangle, \\
A_3^{-}(p_a,p_b,p_c,p_d,p_e,p_f) = {}& A_3^{+}(p_b,p_a,p_c,p_d,p_e,p_f).
\end{aligned} \tag{2.12}$$

The spinor products are defined by

$$\langle pq\rangle = \epsilon^{AB} p_A q_B = 2\sqrt{p_0 q_0}\left[\mathrm{e}^{-\mathrm{i}\phi_p}\cos\frac{\theta_p}{2}\sin\frac{\theta_q}{2} - \mathrm{e}^{-\mathrm{i}\phi_q}\cos\frac{\theta_q}{2}\sin\frac{\theta_p}{2}\right], \tag{2.13}$$

where p_A, q_A are the associated momentum spinors for the momenta

$$\begin{aligned}
p^\mu &= p_0(1, \sin\theta_p\cos\phi_p, \sin\theta_p\sin\phi_p, \cos\theta_p), \\
q^\mu &= p_0(1, \sin\theta_q\cos\phi_q, \sin\theta_q\sin\phi_q, \cos\theta_q).
\end{aligned} \tag{2.14}$$

Incoming fermions are turned into outgoing ones by crossing, which is performed by inverting the corresponding fermion momenta and helicities. If the generic functions are called with negative momenta $-p$, $-q$, it is understood that only the complex conjugate spinor products get the corresponding sign change. We illustrate this by simple examples:

$$\begin{aligned}
A(p,q) = \langle pq\rangle &= A(p,-q) = A(-p,q) = A(-p,-q), \\
B(p,q) = \langle pq\rangle^* &= -B(p,-q) = -B(-p,q) = B(-p,-q).
\end{aligned} \tag{2.15}$$

We have checked the results for the generic diagrams against those of Ref. [16] and found agreement.

Using the results for the generic diagrams of Figure 1, the helicity amplitudes for all possible processes involving six external fermions can be built up. It is convenient to construct first the amplitudes for the process types CC(a) and NC(a) (see Section 2.2) in terms of the generic functions (2.8) and (2.9), because these amplitudes are the basic subamplitudes of the other channels. The full amplitude for each process type can be built up from those subamplitudes by appropriate substitutions and linear combinations.

We first list the helicity amplitudes for the CC processes:

$$\begin{aligned}
&\mathcal{M}_{\mathrm{CCa}}^{\sigma_+,\sigma_-,\sigma_1,\sigma_2,\sigma_3,\sigma_4}(p_+,p_-,k_1,k_2,k_3,k_4)\\
&\quad= \mathcal{M}_{WW}^{\sigma_+,\sigma_-,-\sigma_1,-\sigma_2,-\sigma_3,-\sigma_4}(p_+,p_-,-k_1,-k_2,-k_3,-k_4)\\
&\qquad+\sum_{V=\gamma,Z}\Big[\quad \mathcal{M}_{VWW}^{\sigma_+,\sigma_-,-\sigma_1,-\sigma_2,-\sigma_3,-\sigma_4}(p_+,p_-,-k_1,-k_2,-k_3,-k_4)\\
&\qquad\qquad+\mathcal{M}_{VW}^{-\sigma_1,-\sigma_2,\sigma_+,\sigma_-,-\sigma_3,-\sigma_4}(-k_1,-k_2,p_+,p_-,-k_3,-k_4)\\
&\qquad\qquad+\mathcal{M}_{VW}^{-\sigma_3,-\sigma_4,\sigma_+,\sigma_-,-\sigma_1,-\sigma_2}(-k_3,-k_4,p_+,p_-,-k_1,-k_2)\\
&\qquad\qquad+\mathcal{M}_{WV}^{-\sigma_1,-\sigma_2,-\sigma_3,-\sigma_4,\sigma_+,\sigma_-}(-k_1,-k_2,-k_3,-k_4,p_+,p_-)\\
&\qquad\qquad+\mathcal{M}_{WV}^{-\sigma_3,-\sigma_4,-\sigma_1,-\sigma_2,\sigma_+,\sigma_-}(-k_3,-k_4,-k_1,-k_2,p_+,p_-)\Big],
\end{aligned}\tag{2.16}$$

$$\begin{aligned}
&\mathcal{M}_{\mathrm{CCb}}^{\sigma_+,\sigma_-,\sigma_1,\sigma_2,\sigma_3,\sigma_4}(p_+,p_-,k_1,k_2,k_3,k_4)\\
&\quad= \quad\mathcal{M}_{\mathrm{CCa}}^{\sigma_+,\sigma_-,\sigma_1,\sigma_2,\sigma_3,\sigma_4}(p_+,p_-,k_1,k_2,k_3,k_4)\\
&\qquad-\mathcal{M}_{\mathrm{CCa}}^{\sigma_+,-\sigma_2,\sigma_1,-\sigma_-,\sigma_3,\sigma_4}(p_+,-k_2,k_1,-p_-,k_3,k_4),
\end{aligned}\tag{2.17}$$

$$\begin{aligned}
&\mathcal{M}_{\mathrm{CCc}}^{\sigma_+,\sigma_-,\sigma_1,\sigma_2,\sigma_3,\sigma_4}(p_+,p_-,k_1,k_2,k_3,k_4)\\
&\quad= \quad\mathcal{M}_{\mathrm{CCa}}^{\sigma_+,\sigma_-,\sigma_1,\sigma_2,\sigma_3,\sigma_4}(p_+,p_-,k_1,k_2,k_3,k_4)\\
&\qquad-\mathcal{M}_{\mathrm{CCa}}^{-\sigma_3,\sigma_-,\sigma_1,\sigma_2,-\sigma_+,\sigma_4}(-k_3,p_-,k_1,k_2,-p_+,k_4).
\end{aligned}\tag{2.18}$$

The ones for the NC processes are given by

$$\begin{aligned}
&\mathcal{M}_{\mathrm{NCa}}^{\sigma_+,\sigma_-,\sigma_1,\sigma_2,\sigma_3,\sigma_4}(p_+,p_-,k_1,k_2,k_3,k_4)\\
&\quad=\sum_{V_1,V_2=\gamma,Z}\Big[\quad \mathcal{M}_{V_1V_2}^{\sigma_+,\sigma_-,-\sigma_1,-\sigma_2,-\sigma_3,-\sigma_4}(p_+,p_-,-k_1,-k_2,-k_3,-k_4)\\
&\qquad\qquad+\mathcal{M}_{V_1V_2}^{\sigma_+,\sigma_-,-\sigma_3,-\sigma_4,-\sigma_1,-\sigma_2}(p_+,p_-,-k_3,-k_4,-k_1,-k_2)\\
&\qquad\qquad+\mathcal{M}_{V_1V_2}^{-\sigma_1,-\sigma_2,\sigma_+,\sigma_-,-\sigma_3,-\sigma_4}(-k_1,-k_2,p_+,p_-,-k_3,-k_4)\\
&\qquad\qquad+\mathcal{M}_{V_1V_2}^{-\sigma_3,-\sigma_4,\sigma_+,\sigma_-,-\sigma_1,-\sigma_2}(-k_3,-k_4,p_+,p_-,-k_1,-k_2)\\
&\qquad\qquad+\mathcal{M}_{V_1V_2}^{-\sigma_1,-\sigma_2,-\sigma_3,-\sigma_4,\sigma_+,\sigma_-}(-k_1,-k_2,-k_3,-k_4,p_+,p_-)\\
&\qquad\qquad+\mathcal{M}_{V_1V_2}^{-\sigma_3,-\sigma_4,-\sigma_1,-\sigma_2,\sigma_+,\sigma_-}(-k_3,-k_4,-k_1,-k_2,p_+,p_-)\Big],
\end{aligned}\tag{2.19}$$

$$\begin{aligned}
&\mathcal{M}_{\mathrm{NCb}}^{\sigma_+,\sigma_-,\sigma_1,\sigma_2,\sigma_3,\sigma_4}(p_+,p_-,k_1,k_2,k_3,k_4)\\
&\quad= \quad\mathcal{M}_{\mathrm{NCa}}^{\sigma_+,\sigma_-,\sigma_1,\sigma_2,\sigma_3,\sigma_4}(p_+,p_-,k_1,k_2,k_3,k_4)\\
&\qquad-\mathcal{M}_{\mathrm{NCa}}^{\sigma_+,\sigma_-,\sigma_3,\sigma_2,\sigma_1,\sigma_4}(p_+,p_-,k_3,k_2,k_1,k_4),
\end{aligned}\tag{2.20}$$

$$
\begin{aligned}
&\mathcal{M}_{\mathrm{NCc}}^{\sigma_+,\sigma_-,\sigma_1,\sigma_2,\sigma_3,\sigma_4}(p_+,p_-,k_1,k_2,k_3,k_4)\\
&\qquad = \quad \mathcal{M}_{\mathrm{NCa}}^{\sigma_+,\sigma_-,\sigma_1,\sigma_2,\sigma_3,\sigma_4}(p_+,p_-,k_1,k_2,k_3,k_4)\\
&\qquad\quad - \mathcal{M}_{\mathrm{NCa}}^{-\sigma_1,\sigma_-,-\sigma_+,\sigma_2,\sigma_3,\sigma_4}(-k_1,p_-,-p_+,k_2,k_3,k_4),
\end{aligned}
\tag{2.21}
$$

$$
\begin{aligned}
&\mathcal{M}_{\mathrm{NCd}}^{\sigma_+,\sigma_-,\sigma_1,\sigma_2,\sigma_3,\sigma_4}(p_+,p_-,k_1,k_2,k_3,k_4)\\
&\qquad = \quad \mathcal{M}_{\mathrm{NCa}}^{\sigma_+,\sigma_-,\sigma_1,\sigma_2,\sigma_3,\sigma_4}(p_+,p_-,k_1,k_2,k_3,k_4)\\
&\qquad\quad - \mathcal{M}_{\mathrm{NCa}}^{\sigma_+,\sigma_-,\sigma_3,\sigma_2,\sigma_1,\sigma_4}(p_+,p_-,k_3,k_2,k_1,k_4)\\
&\qquad\quad - \mathcal{M}_{\mathrm{NCa}}^{-\sigma_1,\sigma_-,-\sigma_+,\sigma_2,\sigma_3,\sigma_4}(-k_1,p_-,-p_+,k_2,k_3,k_4)\\
&\qquad\quad - \mathcal{M}_{\mathrm{NCa}}^{-\sigma_3,\sigma_-,\sigma_1,\sigma_2,-\sigma_+,\sigma_4}(-k_3,p_-,k_1,k_2,-p_+,k_4)\\
&\qquad\quad + \mathcal{M}_{\mathrm{NCa}}^{-\sigma_1,\sigma_-,\sigma_3,\sigma_2,-\sigma_+,\sigma_4}(-k_1,p_-,k_3,k_2,-p_+,k_4)\\
&\qquad\quad + \mathcal{M}_{\mathrm{NCa}}^{-\sigma_3,\sigma_-,-\sigma_+,\sigma_2,\sigma_1,\sigma_4}(-k_3,p_-,-p_+,k_2,k_1,k_4).
\end{aligned}
\tag{2.22}
$$

Finally, the helicity amplitudes for reactions of mixed CC/NC type read

$$
\begin{aligned}
&\mathcal{M}_{\mathrm{CC/NCa}}^{\sigma_+,\sigma_-,\sigma_1,\sigma_2,\sigma_3,\sigma_4}(p_+,p_-,k_1,k_2,k_3,k_4)\\
&\qquad = \quad \mathcal{M}_{\mathrm{NCa}}^{\sigma_+,\sigma_-,\sigma_1,\sigma_2,\sigma_3,\sigma_4}(p_+,p_-,k_1,k_2,k_3,k_4)\\
&\qquad\quad - \mathcal{M}_{\mathrm{CCa}}^{\sigma_+,\sigma_-,\sigma_1,\sigma_4,\sigma_3,\sigma_2}(p_+,p_-,k_1,k_4,k_3,k_2),
\end{aligned}
\tag{2.23}
$$

$$
\begin{aligned}
&\mathcal{M}_{\mathrm{CC/NCb}}^{\sigma_+,\sigma_-,\sigma_1,\sigma_2,\sigma_3,\sigma_4}(p_+,p_-,k_1,k_2,k_3,k_4)\\
&\qquad = \quad \mathcal{M}_{\mathrm{NCa}}^{\sigma_+,\sigma_-,\sigma_1,\sigma_2,\sigma_3,\sigma_4}(p_+,p_-,k_1,k_2,k_3,k_4)\\
&\qquad\quad - \mathcal{M}_{\mathrm{CCa}}^{-\sigma_3,-\sigma_4,\sigma_1,-\sigma_-,-\sigma_+,\sigma_2}(-k_3,-k_4,k_1,-p_-,-p_+,k_2),
\end{aligned}
\tag{2.24}
$$

$$
\begin{aligned}
&\mathcal{M}_{\mathrm{CC/NCc}}^{\sigma_+,\sigma_-,\sigma_1,\sigma_2,\sigma_3,\sigma_4}(p_+,p_-,k_1,k_2,k_3,k_4)\\
&\qquad = \quad \mathcal{M}_{\mathrm{NCa}}^{\sigma_+,\sigma_-,\sigma_1,\sigma_2,\sigma_3,\sigma_4}(p_+,p_-,k_1,k_2,k_3,k_4)\\
&\qquad\quad - \mathcal{M}_{\mathrm{NCa}}^{\sigma_+,\sigma_-,\sigma_3,\sigma_2,\sigma_1,\sigma_4}(p_+,p_-,k_3,k_2,k_1,k_4)\\
&\qquad\quad - \mathcal{M}_{\mathrm{CCa}}^{-\sigma_1,-\sigma_2,-\sigma_+,\sigma_4,\sigma_3,-\sigma_-}(-k_1,-k_2,k_3,-p_-,-p_+,k_4)\\
&\qquad\quad + \mathcal{M}_{\mathrm{CCa}}^{-\sigma_1,-\sigma_4,-\sigma_+,\sigma_2,\sigma_3,-\sigma_-}(-k_1,-k_4,k_3,-p_-,-p_+,k_2)\\
&\qquad\quad + \mathcal{M}_{\mathrm{CCa}}^{-\sigma_3,-\sigma_2,-\sigma_+,\sigma_4,\sigma_1,-\sigma_-}(-k_3,-k_2,k_1,-p_-,-p_+,k_4)\\
&\qquad\quad - \mathcal{M}_{\mathrm{CCa}}^{-\sigma_3,-\sigma_4,-\sigma_+,\sigma_2,\sigma_1,-\sigma_-}(-k_3,-k_4,k_1,-p_-,-p_+,k_2),
\end{aligned}
\tag{2.25}
$$

$$
\begin{aligned}
&\mathcal{M}_{\mathrm{CC/NCd}}^{\sigma_+,\sigma_-,\sigma_1,\sigma_2,\sigma_3,\sigma_4}(p_+,p_-,k_1,k_2,k_3,k_4)\\
&\qquad = \quad \mathcal{M}_{\mathrm{NCa}}^{\sigma_+,\sigma_-,\sigma_1,\sigma_2,\sigma_3,\sigma_4}(p_+,p_-,k_1,k_2,k_3,k_4)\\
&\qquad\quad - \mathcal{M}_{\mathrm{NCa}}^{-\sigma_3,\sigma_-,\sigma_1,\sigma_2,-\sigma_+,\sigma_4}(-k_3,p_-,k_1,k_2,-p_+,k_4)\\
&\qquad\quad - \mathcal{M}_{\mathrm{CCa}}^{\sigma_+,\sigma_-,\sigma_1,\sigma_4,\sigma_3,\sigma_2}(p_+,p_-,k_1,k_4,k_3,k_2)\\
&\qquad\quad + \mathcal{M}_{\mathrm{CCa}}^{\sigma_+,-\sigma_4,\sigma_1,-\sigma_-,\sigma_3,\sigma_2}(p_+,-k_4,k_1,-p_-,k_3,k_2)\\
&\qquad\quad + \mathcal{M}_{\mathrm{CCa}}^{-\sigma_3,\sigma_-,\sigma_1,\sigma_4,-\sigma_+,\sigma_2}(-k_3,p_-,k_1,k_4,-p_+,k_2)\\
&\qquad\quad - \mathcal{M}_{\mathrm{CCa}}^{-\sigma_3,-\sigma_4,\sigma_1,-\sigma_-,-\sigma_+,\sigma_2}(-k_3,-k_4,k_1,-p_-,-p_+,k_2).
\end{aligned}
\tag{2.26}
$$

The relative signs between contributions of the basic subamplitudes $\mathcal{M}_{\mathrm{CCa}}$ and $\mathcal{M}_{\mathrm{NCa}}$ to the full matrix elements account for the sign changes resulting from interchanging external fermion lines.

For the CC reactions, the amplitudes $\mathcal{M}_{\mathrm{CCa}}$ are the smallest gauge-invariant subset of diagrams [24]. In the case of NC reactions, the amplitudes $\mathcal{M}_{\mathrm{NCa}}$ are composed of three separately gauge-invariant subamplitudes consisting of the first two lines, the two lines in the middle, and the last two lines of (2.19).

2.3.2 Hadronic final states

Next we inspect purely hadronic final states, i.e. the cases where all final-state fermions f_i are quarks. This concerns only the channels CC(a), NC(a), NC(b), and CC/NC(a) given in Section 2.2. The colour structure of the quarks leads to two kinds of modifications. Firstly, the summation of the squared amplitudes over the colour degrees of freedom can become non-trivial, and secondly, the possibility of virtual-gluon exchange between the quarks has to be taken into account. More precisely, there are diagrams of type (a) in Figure 1 in which one of the gauge bosons $V_{1,2}$ is a gluon. The other gauge boson of $V_{1,2}$ can only be a photon or Z boson, since this boson has to couple to the incoming $\mathrm{e}^+\mathrm{e}^-$ pair. Consequently, there is an impact of gluon-exchange diagrams only for the channels NC(a), NC(b), and CC/NC(a), but not for CC(a). This can be easily seen by inspecting the generic diagrams in Figure 1: the presence of a gluon exchange requires two quark–antiquark pairs $q\bar{q}$ in the final state.

We first inspect the colour structure of the purely electroweak diagrams. Since the colour structure of each diagram contributing to the basic channels CC(a) and NC(a) is the same, the corresponding amplitudes factorize into a simple colour part and the "colour-singlet amplitudes" $\mathcal{M}_{\mathrm{CCa}}$ and $\mathcal{M}_{\mathrm{NCa}}$, given in (2.16) and (2.19), respectively. The amplitudes for NC(b) and CC/NC(a) are composed from the ones of CC(a) and NC(a) in a way that is analogous to the singlet case, but now the colour indices c_i of the quarks f_i have to be taken into account. Indicating the electroweak amplitudes for fully hadronic final states by "had, ew", and writing colour indices explicitly, we get

$$\begin{aligned}
&\mathcal{M}^{\sigma_+,\sigma_-,\sigma_1,\sigma_2,\sigma_3,\sigma_4}_{\mathrm{CCa,had,ew},c_1,c_2,c_3,c_4}(p_+,p_-,k_1,k_2,k_3,k_4)\\
&\qquad = \mathcal{M}^{\sigma_+,\sigma_-,\sigma_1,\sigma_2,\sigma_3,\sigma_4}_{\mathrm{CCa}}(p_+,p_-,k_1,k_2,k_3,k_4)\,\delta_{c_1c_2}\delta_{c_3c_4}, \qquad (2.27)
\end{aligned}$$

$$\begin{aligned}
&\mathcal{M}^{\sigma_+,\sigma_-,\sigma_1,\sigma_2,\sigma_3,\sigma_4}_{\mathrm{NCa,had,ew},c_1,c_2,c_3,c_4}(p_+,p_-,k_1,k_2,k_3,k_4)\\
&\qquad = \mathcal{M}^{\sigma_+,\sigma_-,\sigma_1,\sigma_2,\sigma_3,\sigma_4}_{\mathrm{NCa}}(p_+,p_-,k_1,k_2,k_3,k_4)\,\delta_{c_1c_2}\delta_{c_3c_4}, \qquad (2.28)
\end{aligned}$$

$$\begin{aligned}
&\mathcal{M}^{\sigma_+,\sigma_-,\sigma_1,\sigma_2,\sigma_3,\sigma_4}_{\mathrm{NCb,had,ew},c_1,c_2,c_3,c_4}(p_+,p_-,k_1,k_2,k_3,k_4)\\
&\qquad = \mathcal{M}^{\sigma_+,\sigma_-,\sigma_1,\sigma_2,\sigma_3,\sigma_4}_{\mathrm{NCa}}(p_+,p_-,k_1,k_2,k_3,k_4)\,\delta_{c_1c_2}\delta_{c_3c_4}\\
&\qquad\quad - \mathcal{M}^{\sigma_+,\sigma_-,\sigma_3,\sigma_2,\sigma_1,\sigma_4}_{\mathrm{NCa}}(p_+,p_-,k_3,k_2,k_1,k_4)\,\delta_{c_3c_2}\delta_{c_1c_4}, \qquad (2.29)
\end{aligned}$$

$$\begin{aligned}
&\mathcal{M}^{\sigma_+,\sigma_-,\sigma_1,\sigma_2,\sigma_3,\sigma_4}_{\mathrm{CC/NCa,had,ew},c_1,c_2,c_3,c_4}(p_+,p_-,k_1,k_2,k_3,k_4)\\
&\qquad = \mathcal{M}^{\sigma_+,\sigma_-,\sigma_1,\sigma_2,\sigma_3,\sigma_4}_{\mathrm{NCa}}(p_+,p_-,k_1,k_2,k_3,k_4)\,\delta_{c_1c_2}\delta_{c_3c_4}\\
&\qquad\quad - \mathcal{M}^{\sigma_+,\sigma_-,\sigma_1,\sigma_4,\sigma_3,\sigma_2}_{\mathrm{CCa}}(p_+,p_-,k_1,k_4,k_3,k_2)\,\delta_{c_1c_4}\delta_{c_3c_2}. \qquad (2.30)
\end{aligned}$$

In the calculation of the gluon-exchange diagrams we can also make use of the "colour-singlet" result (2.8) for the generic diagram (a) of Figure 1, after splitting off the colour structure appropriately. Since each of these diagrams involves exactly one internal gluon, exchanged by the two quark lines, the corresponding matrix elements can be deduced in a simple way from the diagrams in which the gluon is replaced by a photon. The gluon-exchange contributions to the channels NC(b) and CC/NC(a) can again be composed from the ones for NC(a). Making use of the auxiliary function

$$\begin{aligned}
&\mathcal{M}_{\mathrm{g}}^{\sigma_+,\sigma_-,\sigma_1,\sigma_2,\sigma_3,\sigma_4}(p_+,p_-,k_1,k_2,k_3,k_4)\\
&\quad = \frac{g_{\mathrm{s}}^2}{Q_1 Q_3 e^2} \sum_{V=\gamma,Z} \Big[\quad \mathcal{M}_{V\gamma}^{-\sigma_1,-\sigma_2,\sigma_+,\sigma_-,-\sigma_3,-\sigma_4}(-k_1,-k_2,p_+,p_-,-k_3,-k_4)\\
&\qquad\qquad + \mathcal{M}_{V\gamma}^{-\sigma_3,-\sigma_4,\sigma_+,\sigma_-,-\sigma_1,-\sigma_2}(-k_3,-k_4,p_+,p_-,-k_1,-k_2)\\
&\qquad\qquad + \mathcal{M}_{\gamma V}^{-\sigma_1,-\sigma_2,-\sigma_3,-\sigma_4,\sigma_+,\sigma_-}(-k_1,-k_2,-k_3,-k_4,p_+,p_-)\\
&\qquad\qquad + \mathcal{M}_{\gamma V}^{-\sigma_3,-\sigma_4,-\sigma_1,-\sigma_2,\sigma_+,\sigma_-}(-k_3,-k_4,-k_1,-k_2,p_+,p_-)\Big], \qquad (2.31)
\end{aligned}$$

where $g_{\mathrm{s}} = \sqrt{4\pi\alpha_{\mathrm{s}}}$ is the strong gauge coupling, the matrix elements involving gluon exchange explicitly read

$$\begin{aligned}
&\mathcal{M}_{\mathrm{NCa,had,gluon},c_1,c_2,c_3,c_4}^{\sigma_+,\sigma_-,\sigma_1,\sigma_2,\sigma_3,\sigma_4}(p_+,p_-,k_1,k_2,k_3,k_4)\\
&\qquad = \quad \mathcal{M}_{\mathrm{g}}^{\sigma_+,\sigma_-,\sigma_1,\sigma_2,\sigma_3,\sigma_4}(p_+,p_-,k_1,k_2,k_3,k_4)\, \tfrac{1}{4}\, \lambda_{c_1c_2}^a \lambda_{c_3c_4}^a, \qquad (2.32)
\end{aligned}$$

$$\begin{aligned}
&\mathcal{M}_{\mathrm{NCb,had,gluon},c_1,c_2,c_3,c_4}^{\sigma_+,\sigma_-,\sigma_1,\sigma_2,\sigma_3,\sigma_4}(p_+,p_-,k_1,k_2,k_3,k_4)\\
&\qquad = \quad \mathcal{M}_{\mathrm{g}}^{\sigma_+,\sigma_-,\sigma_1,\sigma_2,\sigma_3,\sigma_4}(p_+,p_-,k_1,k_2,k_3,k_4)\, \tfrac{1}{4}\, \lambda_{c_1c_2}^a \lambda_{c_3c_4}^a\\
&\qquad\quad - \mathcal{M}_{\mathrm{g}}^{\sigma_+,\sigma_-,\sigma_3,\sigma_2,\sigma_1,\sigma_4}(p_+,p_-,k_3,k_2,k_1,k_4)\, \tfrac{1}{4}\, \lambda_{c_3c_2}^a \lambda_{c_1c_4}^a, \qquad (2.33)
\end{aligned}$$

$$\begin{aligned}
&\mathcal{M}_{\mathrm{CC/NCa,had,gluon},c_1,c_2,c_3,c_4}^{\sigma_+,\sigma_-,\sigma_1,\sigma_2,\sigma_3,\sigma_4}(p_+,p_-,k_1,k_2,k_3,k_4)\\
&\qquad = \quad \mathcal{M}_{\mathrm{g}}^{\sigma_+,\sigma_-,\sigma_1,\sigma_2,\sigma_3,\sigma_4}(p_+,p_-,k_1,k_2,k_3,k_4)\, \tfrac{1}{4}\, \lambda_{c_1c_2}^a \lambda_{c_3c_4}^a. \qquad (2.34)
\end{aligned}$$

The colour structure is easily evaluated by making use of the completeness relation $\lambda_{ij}^a \lambda_{kl}^a = -\frac{2}{3}\delta_{ij}\delta_{kl} + 2\delta_{il}\delta_{jk}$ for the Gell-Mann matrices λ_{ij}^a.

The complete matrix elements for the fully hadronic channels result from the sum of the purely electroweak and the gluon-exchange contributions,

$$\mathcal{M}_{\dots,\mathrm{had},c_1,c_2,c_3,c_4}^{\sigma_+,\sigma_-,\sigma_1,\sigma_2,\sigma_3,\sigma_4} = \mathcal{M}_{\dots,\mathrm{had,ew},c_1,c_2,c_3,c_4}^{\sigma_+,\sigma_-,\sigma_1,\sigma_2,\sigma_3,\sigma_4} + \mathcal{M}_{\dots,\mathrm{had,gluon},c_1,c_2,c_3,c_4}^{\sigma_+,\sigma_-,\sigma_1,\sigma_2,\sigma_3,\sigma_4}. \qquad (2.35)$$

The gluon-exchange contributions are separately gauge-invariant.

For clarity, we explicitly write down the colour-summed squared matrix elements for the fully hadronic channels. Abbreviating $\mathcal{M}_{\dots}^{\sigma_+,\sigma_-,\sigma_a,\sigma_b,\sigma_c,\sigma_d}(p_+,p_-,k_a,k_b,k_c,k_d)$ by $\mathcal{M}_{\dots}(a,b,c,d)$ we obtain

$$\sum_{\mathrm{colour}} |\mathcal{M}_{\mathrm{CCa,had}}(1,2,3,4)|^2 = 9|\mathcal{M}_{\mathrm{CCa}}(1,2,3,4)|^2, \qquad (2.36)$$

$$\sum_{\mathrm{colour}} |\mathcal{M}_{\mathrm{NCa,had}}(1,2,3,4)|^2 = 9|\mathcal{M}_{\mathrm{NCa}}(1,2,3,4)|^2 + 2|\mathcal{M}_{\mathrm{g}}(1,2,3,4)|^2, \qquad (2.37)$$

$$\begin{aligned}
&\sum_{\mathrm{colour}} |\mathcal{M}_{\mathrm{NCb,had}}(1,2,3,4)|^2\\
&\quad = 9|\mathcal{M}_{\mathrm{NCa}}(1,2,3,4)|^2 + 9|\mathcal{M}_{\mathrm{NCa}}(3,2,1,4)|^2 - 6\,\mathrm{Re}\left\{\mathcal{M}_{\mathrm{NCa}}(1,2,3,4)\mathcal{M}_{\mathrm{NCa}}^*(3,2,1,4)\right\}
\end{aligned}$$

$$
\begin{aligned}
&+ 2|\mathcal{M}_{\mathrm{g}}(1,2,3,4)|^2 + 2|\mathcal{M}_{\mathrm{g}}(3,2,1,4)|^2 + \tfrac{4}{3}\,\mathrm{Re}\,\{\mathcal{M}_{\mathrm{g}}(1,2,3,4)\mathcal{M}^*_{\mathrm{g}}(3,2,1,4)\} \\
&- 8\,\mathrm{Re}\,\{\mathcal{M}_{\mathrm{NCa}}(1,2,3,4)\mathcal{M}^*_{\mathrm{g}}(3,2,1,4)\} - 8\,\mathrm{Re}\,\{\mathcal{M}_{\mathrm{NCa}}(3,2,1,4)\mathcal{M}^*_{\mathrm{g}}(1,2,3,4)\},
\end{aligned}
\tag{2.38}
$$

$$
\begin{aligned}
&\sum_{\mathrm{colour}} |\mathcal{M}_{\mathrm{CC/NCa,had}}(1,2,3,4)|^2 \\
&= 9|\mathcal{M}_{\mathrm{NCa}}(1,2,3,4)|^2 + 9|\mathcal{M}_{\mathrm{CCa}}(1,4,3,2)|^2 - 6\,\mathrm{Re}\,\{\mathcal{M}_{\mathrm{NCa}}(1,2,3,4)\mathcal{M}^*_{\mathrm{CCa}}(1,4,3,2)\} \\
&\quad + 2|\mathcal{M}_{\mathrm{g}}(1,2,3,4)|^2 - 8\,\mathrm{Re}\,\{\mathcal{M}_{\mathrm{CCa}}(1,4,3,2)\mathcal{M}^*_{\mathrm{g}}(1,2,3,4)\}.
\end{aligned}
\tag{2.39}
$$

Owing to the colour structure of the diagrams, a non-zero interference between purely electroweak and gluon-exchange contributions is only possible if the four final-state fermions can be combined into one single closed fermion line in the squared diagram. This implies that fermion pairs must couple to different resonances in the electroweak and the gluon-exchange diagrams, leading to a global suppression of such interference effects in the phase-space integration (see Section 4.5).

2.4 Generic functions and amplitudes for $\mathrm{e}^+\mathrm{e}^- \to 4f\gamma$

The generic functions for $\mathrm{e}^+\mathrm{e}^- \to 4f\gamma$ can be constructed in a similar way. The idea is to combine the contributions of all those graphs to one generic function that reduce to the same graph after removing the radiated photon. These combined contributions to $\mathrm{e}^+\mathrm{e}^- \to 4f\gamma$ are classified in the same way as the diagrams for the corresponding process $\mathrm{e}^+\mathrm{e}^- \to 4f$, i.e. the graphs of Figure 1 also represent the generic functions for $\mathrm{e}^+\mathrm{e}^- \to 4f\gamma$. Finally, all amplitudes for $\mathrm{e}^+\mathrm{e}^- \to 4f\gamma$ can again be constructed from only two generic functions. Note that the number of individual Feynman diagrams ranges between 14 and 1008 for the various processes. We note that the generic functions can in fact be used to construct the amplitudes for all processes involving exactly six external fermions and one external photon, such as $\mathrm{e}^-\mathrm{e}^- \to 4f\gamma$ and $\mathrm{e}\gamma \to 5f$.

As a virtue of this approach, the so-defined generic functions fulfill the QED Ward identity for the external photon, i.e. replacing the photon polarization vector by the photon momentum yields zero for each generic function. This is simply a consequence of electromagnetic charge conservation. Consequently, in the actual calculation in the WvdW formalism the gauge spinor of the photon drops out in each contribution separately.

Assuming the external fermions as incoming and the photon as outgoing, the generic functions read

$$
\begin{aligned}
&\mathcal{M}^{\sigma_a,\sigma_b,\sigma_c,\sigma_d,\sigma_e,\sigma_f,\lambda}_{V_1V_2}(Q_a,Q_b,Q_c,Q_d,Q_e,Q_f,p_a,p_b,p_c,p_d,p_e,p_f,k) \\
&\quad = -4\sqrt{2}e^5\delta_{\sigma_a,-\sigma_b}\delta_{\sigma_c,-\sigma_d}\delta_{\sigma_e,-\sigma_f}\, g^{\sigma_b}_{V_1\bar{f}_af_g}g^{\sigma_b}_{V_2\bar{f}_gf_b}g^{\sigma_d}_{V_1\bar{f}_cf_d}g^{\sigma_f}_{V_2\bar{f}_ef_f} \\
&\qquad \times A_2^{\sigma_a,\sigma_c,\sigma_e,\lambda}(Q_a,Q_b,Q_c,Q_d,Q_e,Q_f,p_a,p_b,p_c,p_d,p_e,p_f,k),
\end{aligned}
\tag{2.40}
$$

$$
\begin{aligned}
&\mathcal{M}^{\sigma_a,\sigma_b,\sigma_c,\sigma_d,\sigma_e,\sigma_f,\lambda}_{VWW}(Q_a,Q_b,Q_c,Q_d,Q_e,Q_f,p_a,p_b,p_c,p_d,p_e,p_f,k) \\
&\quad = -4\sqrt{2}e^5\delta_{\sigma_a,-\sigma_b}\delta_{\sigma_c,+}\delta_{\sigma_d,-}\delta_{\sigma_e,+}\delta_{\sigma_f,-}\,(Q_c-Q_d)g_{VWW}g^{\sigma_b}_{V\bar{f}_af_b}g^{-}_{W\bar{f}_cf_d}g^{-}_{W\bar{f}_ef_f} \\
&\qquad \times A_3^{\sigma_a,\lambda}(Q_a,Q_b,Q_c,Q_d,Q_e,Q_f,p_a,p_b,p_c,p_d,p_e,p_f,k),
\end{aligned}
\tag{2.41}
$$

with the auxiliary functions

$$
\begin{aligned}
& A_2^{++++}(Q_a,Q_b,Q_c,Q_d,Q_e,Q_f,p_a,p_b,p_c,p_d,p_e,p_f,k) = -\langle p_a p_c\rangle \Big\{ \\
&\quad P_{V_1}(p_c+p_d)P_{V_2}(p_e+p_f) \\
&\qquad \times \Big[\frac{\langle p_b p_f\rangle^*}{\langle p_a k\rangle} \Big(\frac{Q_c-Q_d}{(p_b+p_e+p_f)^2}\frac{\langle p_a p_c\rangle}{\langle p_c k\rangle}(\langle p_b p_d\rangle^*\langle p_b p_e\rangle + \langle p_d p_f\rangle^*\langle p_e p_f\rangle) \\
&\qquad\qquad + \frac{Q_f-Q_e}{(p_a+p_c+p_d)^2}\frac{\langle p_a p_e\rangle}{\langle p_e k\rangle}(\langle p_a p_d\rangle^*\langle p_a p_e\rangle + \langle p_c p_d\rangle^*\langle p_c p_e\rangle)\Big) \\
&\qquad + \frac{Q_b(\langle p_a p_d\rangle^*\langle p_a p_e\rangle + \langle p_c p_d\rangle^*\langle p_c p_e\rangle)(\langle p_b p_f\rangle^*\langle p_a p_b\rangle - \langle p_f k\rangle^*\langle p_a k\rangle)}{(p_a+p_c+p_d)^2\langle p_a k\rangle\langle p_b k\rangle} \\
&\qquad + \frac{(Q_a+Q_c-Q_d)\langle p_b p_f\rangle^*\langle p_c p_d\rangle^*\langle p_a p_c\rangle(\langle p_b k\rangle^*\langle p_b p_e\rangle - \langle p_f k\rangle^*\langle p_e p_f\rangle)}{(p_a+p_c+p_d)^2(p_b+p_e+p_f)^2\langle p_a k\rangle}\Big] \\
&\quad - \frac{Q_d-(Q_c-Q_d)2(p_d\cdot k)P_{V_1}(p_c+p_d)}{(p_b+p_e+p_f)^2}P_{V_1}(p_c+p_d-k)P_{V_2}(p_e+p_f)\langle p_b p_f\rangle^* \\
&\qquad \times \frac{\langle p_c p_d\rangle(\langle p_b p_d\rangle^*\langle p_b p_e\rangle + \langle p_d p_f\rangle^*\langle p_e p_f\rangle) + \langle p_c k\rangle(\langle p_b k\rangle^*\langle p_b p_e\rangle - \langle p_f k\rangle^*\langle p_e p_f\rangle)}{\langle p_c k\rangle\langle p_d k\rangle} \\
&\quad + \frac{Q_f-(Q_e-Q_f)2(p_f\cdot k)P_{V_2}(p_e+p_f)}{(p_a+p_c+p_d)^2}P_{V_1}(p_c+p_d)P_{V_2}(p_e+p_f-k) \\
&\qquad \times \frac{(\langle p_b p_f\rangle^*\langle p_e p_f\rangle + \langle p_b k\rangle^*\langle p_e k\rangle)(\langle p_a p_d\rangle^*\langle p_a p_e\rangle + \langle p_c p_d\rangle^*\langle p_c p_e\rangle)}{\langle p_e k\rangle\langle p_f k\rangle}\Big\}, \\
& A_2^{++-+}(Q_a,Q_b,Q_c,Q_d,Q_e,Q_f,p_a,p_b,p_c,p_d,p_e,p_f,k) \\
&\quad = A_2^{++++}(Q_a,Q_b,Q_c,Q_d,-Q_f,-Q_e,p_a,p_b,p_c,p_d,p_f,p_e,k), \\
& A_2^{+-++}(Q_a,Q_b,Q_c,Q_d,Q_e,Q_f,p_a,p_b,p_c,p_d,p_e,p_f,k) \\
&\quad = A_2^{++++}(Q_a,Q_b,-Q_d,-Q_c,Q_e,Q_f,p_a,p_b,p_d,p_c,p_e,p_f,k), \\
& A_2^{+--+}(Q_a,Q_b,Q_c,Q_d,Q_e,Q_f,p_a,p_b,p_c,p_d,p_e,p_f,k) \\
&\quad = A_2^{++++}(Q_a,Q_b,-Q_d,-Q_c,-Q_f,-Q_e,p_a,p_b,p_d,p_c,p_f,p_e,k), \\
& A_2^{-+++}(Q_a,Q_b,Q_c,Q_d,Q_e,Q_f,p_a,p_b,p_c,p_d,p_e,p_f,k) \\
&\quad = A_2^{++++}(Q_b,Q_a,-Q_e,-Q_f,-Q_c,-Q_d,p_b,p_a,p_e,p_f,p_c,p_d,k), \\
& A_2^{-+-+}(Q_a,Q_b,Q_c,Q_d,Q_e,Q_f,p_a,p_b,p_c,p_d,p_e,p_f,k) \\
&\quad = A_2^{++++}(Q_b,Q_a,Q_f,Q_e,-Q_c,-Q_d,p_b,p_a,p_f,p_e,p_c,p_d,k), \\
& A_2^{--++}(Q_a,Q_b,Q_c,Q_d,Q_e,Q_f,p_a,p_b,p_c,p_d,p_e,p_f,k) \\
&\quad = A_2^{++++}(Q_b,Q_a,-Q_e,-Q_f,Q_d,Q_c,p_b,p_a,p_e,p_f,p_d,p_c,k), \\
& A_2^{---+}(Q_a,Q_b,Q_c,Q_d,Q_e,Q_f,p_a,p_b,p_c,p_d,p_e,p_f,k) \\
&\quad = A_2^{++++}(Q_b,Q_a,Q_f,Q_e,Q_d,Q_c,p_b,p_a,p_f,p_e,p_d,p_c,k), \\
& A_2^{\sigma_a,\sigma_c,\sigma_d,-}(Q_a,Q_b,Q_c,Q_d,Q_e,Q_f,p_a,p_b,p_c,p_d,p_e,p_f,k) \qquad (2.42) \\
&\quad = \Big(A_2^{-\sigma_a,-\sigma_c,-\sigma_d,+}(Q_a,Q_b,Q_c,Q_d,Q_e,Q_f,p_a,p_b,p_c,p_d,p_e,p_f,k)\Big)^*\Big|_{P_{V_{1,2}}(p)\to P^*_{V_{1,2}}(p)},
\end{aligned}
$$

and

$$
\begin{aligned}
&A_3^{++}(Q_a,Q_b,Q_c,Q_d,Q_e,Q_f,p_a,p_b,p_c,p_d,p_e,p_f,k)\\
&\quad= P_V(p_a+p_b)P_W(p_c+p_d)P_W(p_e+p_f)\frac{(Q_c-Q_d)\langle p_cp_e\rangle}{\langle p_ck\rangle\langle p_ek\rangle}\\
&\qquad\quad\times\big(\langle p_bp_d\rangle^*\langle p_bp_f\rangle^*\langle p_ap_b\rangle\langle p_cp_e\rangle + \langle p_bp_d\rangle^*\langle p_dp_f\rangle^*\langle p_ap_e\rangle\langle p_cp_d\rangle\\
&\qquad\qquad + \langle p_bp_f\rangle^*\langle p_dp_f\rangle^*\langle p_ap_c\rangle\langle p_ep_f\rangle\big)\\
&\qquad + P_V(p_a+p_b-k)P_W(p_c+p_d)P_W(p_e+p_f)\frac{Q_b}{\langle p_ak\rangle\langle p_bk\rangle}\\
&\qquad\quad\times\big\{\langle p_dp_f\rangle^*\big[\langle p_ap_e\rangle\langle p_cp_d\rangle(\langle p_bp_d\rangle^*\langle p_ap_b\rangle - \langle p_dk\rangle^*\langle p_ak\rangle)\\
&\qquad\qquad\qquad + \langle p_ap_c\rangle\langle p_ep_f\rangle(\langle p_bp_f\rangle^*\langle p_ap_b\rangle - \langle p_fk\rangle^*\langle p_ak\rangle)\big]\\
&\qquad\qquad + \langle p_cp_e\rangle(\langle p_bp_d\rangle^*\langle p_ap_b\rangle - \langle p_dk\rangle^*\langle p_ak\rangle)(\langle p_bp_f\rangle^*\langle p_ap_b\rangle - \langle p_fk\rangle^*\langle p_ak\rangle)\big\}\\
&\qquad + P_V(p_a+p_b)P_W(p_c+p_d-k)P_W(p_e+p_f)\frac{Q_d-(Q_c-Q_d)2(p_d\cdot k)P_W(p_c+p_d)}{\langle p_ck\rangle\langle p_dk\rangle}\\
&\qquad\quad\times\big\{\langle p_bp_f\rangle^*\big[\langle p_ap_c\rangle\langle p_ep_f\rangle(\langle p_dp_f\rangle^*\langle p_cp_d\rangle - \langle p_fk\rangle^*\langle p_ck\rangle)\\
&\qquad\qquad\qquad + \langle p_cp_e\rangle\langle p_ap_b\rangle(\langle p_bp_d\rangle^*\langle p_cp_d\rangle + \langle p_bk\rangle^*\langle p_ck\rangle)\big]\\
&\qquad\qquad + \langle p_ap_e\rangle(\langle p_dp_f\rangle^*\langle p_cp_d\rangle - \langle p_fk\rangle^*\langle p_ck\rangle)(\langle p_bp_d\rangle^*\langle p_cp_d\rangle + \langle p_bk\rangle^*\langle p_ck\rangle)\big\}\\
&\qquad + P_V(p_a+p_b)P_W(p_c+p_d)P_W(p_e+p_f-k)\frac{Q_f+(Q_f-Q_e)2(p_f\cdot k)P_W(p_e+p_f)}{\langle p_ek\rangle\langle p_fk\rangle}\\
&\qquad\quad\times\big\{\langle p_bp_d\rangle^*\big[\langle p_cp_e\rangle\langle p_ap_b\rangle(\langle p_bp_f\rangle^*\langle p_ep_f\rangle + \langle p_bk\rangle^*\langle p_ek\rangle)\\
&\qquad\qquad\qquad + \langle p_ap_e\rangle\langle p_cp_d\rangle(\langle p_dp_f\rangle^*\langle p_ep_f\rangle + \langle p_dk\rangle^*\langle p_ek\rangle)\big]\\
&\qquad\qquad + \langle p_ap_c\rangle(\langle p_bp_f\rangle^*\langle p_ep_f\rangle + \langle p_bk\rangle^*\langle p_ek\rangle)(\langle p_dp_f\rangle^*\langle p_ep_f\rangle + \langle p_dk\rangle^*\langle p_ek\rangle)\big\},\\
&A_3^{-+}(Q_a,Q_b,Q_c,Q_d,Q_e,Q_f,p_a,p_b,p_c,p_d,p_e,p_f,k)\\
&\quad= A_3^{++}(-Q_b,-Q_a,Q_c,Q_d,Q_e,Q_f,p_b,p_a,p_c,p_d,p_e,p_f,k),\\
&A_3^{\sigma_a,-}(Q_a,Q_b,Q_c,Q_d,Q_e,Q_f,p_a,p_b,p_c,p_d,p_e,p_f,k)\\
&\quad= \Big(A_3^{-\sigma_a,+}(Q_a,Q_b,-Q_d,-Q_c,-Q_f,-Q_e,p_a,p_b,p_d,p_c,p_f,p_e,k)\Big)^*\Big|_{P_{V,W}(p)\to P^*_{V,W}(p)}.
\end{aligned}
\tag{2.43}
$$

The replacements $P_V \to P_V^*$ after the complex conjugation in the last lines of (2.43) and (2.44) ensure that the vector-boson propagators remain unaffected. Note that the vector-boson masses do not enter explicitly in the above results, but only via P_V. In gauges such as the 't Hooft–Feynman or the unitary gauge this feature is obtained only after combining different Feynman graphs for $\mathrm{e}^+\mathrm{e}^- \to 4f\gamma$; in the non-linear gauge (2.3) this is the case diagram by diagram.

The helicity amplitudes for $\mathrm{e}^+\mathrm{e}^- \to 4f\gamma$ follow from the generic functions $\mathcal{M}_{V_1V_2}$ and $\mathcal{M}_{VWW}$ of (2.41) in exactly the same way as described in Section 2.3 for $\mathrm{e}^+\mathrm{e}^- \to 4f$. This holds also for the gluon-exchange matrix elements and for the colour factors. Moreover, the classification of gauge-invariant sets of diagrams for $\mathrm{e}^+\mathrm{e}^- \to 4f$ immediately yields such sets for $\mathrm{e}^+\mathrm{e}^- \to 4f\gamma$, if the additional photon is attached to all graphs of a set in all possible ways.

We have checked analytically that the electromagnetic Ward identity for the external photon is fulfilled for each generic contribution separately. In addition, we have numerically compared the amplitudes for all processes with amplitudes generated by *Madgraph*

[25] for zero width of the vector bosons and found complete agreement. We could not compare our results with *Madgraph* for finite width, because *Madgraph* uses the unitary gauge for massive vector-boson propagators and the ‘t Hooft–Feynman gauge for the photon propagators, while we are using the non-linear gauge (2.3). Therefore, the matrix elements differ after introduction of finite vector-boson widths. While the calculation with *Madgraph* is fully automized, in our calculation we have full control over the matrix element and can, in particular, investigate various implementations of the finite width.

A comparison of our results with those of Refs. [10, 11], which include only the matrix elements that involve two resonant W bosons, immediately reveals the virtues of our generic approach.

2.5 Implementation of finite gauge-boson widths

We have implemented the finite widths of the W and Z bosons in different ways:

- *fixed width* in all propagators: $P_V(p) = [p^2 - M_\mathrm{V}^2 + \mathrm{i}M_\mathrm{V}\Gamma_\mathrm{V}]^{-1}$,
- *running width* in time-like propagators: $P_V(p) = [p^2 - M_\mathrm{V}^2 + \mathrm{i}p^2(\Gamma_\mathrm{V}/M_\mathrm{V})\theta(p^2)]^{-1}$,
- *complex-mass scheme:* complex gauge-boson masses everywhere, i.e. $\sqrt{M_V^2 - \mathrm{i}M_V\Gamma_V}$ instead of M_V in the propagators and in the couplings. This results, in particular, in a constant width in all propagators,

  $$P_V(p) = [p^2 - M_\mathrm{V}^2 + \mathrm{i}M_\mathrm{V}\Gamma_V]^{-1}, \tag{2.44}$$

  and in a complex weak mixing angle:

  $$c_\mathrm{w}^2 = 1 - s_\mathrm{w}^2 = \frac{M_\mathrm{W}^2 - \mathrm{i}M_\mathrm{W}\Gamma_\mathrm{W}}{M_\mathrm{Z}^2 - \mathrm{i}M_\mathrm{Z}\Gamma_\mathrm{Z}}. \tag{2.45}$$

The virtues and drawbacks of the first two schemes have been discussed in Ref. [26]. Both violate SU(2) gauge invariance, the running width also U(1) gauge invariance. The complex-mass scheme obeys all Ward identities[1] and thus gives a consistent description of the finite-width effects in any tree-level calculation. While the complex-mass scheme works in general, it is particularly simple for $\mathrm{e}^+\mathrm{e}^- \to 4f\gamma$ in the non-linear gauge (2.3). In this case, no couplings involving explicit gauge-boson masses appear, and it is sufficient to introduce the finite gauge-boson widths in the propagators [cf. (2.44)] and to introduce the complex weak mixing angle (2.45) in the couplings. We note that a generalization of this scheme to higher orders requires to introduce complex mass counterterms in order to compensate for the complex masses in the propagators [28]. We did not consider the fermion-loop scheme [26, 29], which is also fully consistent for lowest-order predictions, since it requires the calculation of fermionic one-loop corrections to $\mathrm{e}^+\mathrm{e}^- \to 4f\gamma$ which is beyond the scope of this work.

---

[1] In the context of electromagnetic gauge invariance, the introduction of a complex mass has been proposed in Ref. [27]

3 The Monte Carlo programs

The cross section for $\mathrm{e}^+\mathrm{e}^- \to 4f(\gamma)$ is given by

$$\mathrm{d}\sigma = \frac{(2\pi)^{4-3n}}{2s}\left[\prod_{i=1}^{n}\mathrm{d}^4k_i\,\delta\left(k_i^2\right)\theta(k_i^0)\right]\delta^{(4)}\left(p_+ + p_- - \sum_{i=1}^{n}k_i\right) \times |\mathcal{M}(p_+,p_-,k_1,\dots,k_n)|^2, \tag{3.1}$$

where $n = 4,5$ is the number of outgoing particles. The helicity amplitudes $\mathcal{M}$ for $\mathrm{e}^+\mathrm{e}^- \to 4f(\gamma)$ have been calculated in Sections 2.3 and 2.4, respectively. The phase-space integration is performed with the help of a Monte Carlo technique, since the Monte Carlo method allows us to calculate a variety of observables simultaneously and to easily implement cuts in order to account for the experimental situation.

The helicity amplitudes in (3.1) exhibit a complicated peaking behaviour in different regions of the integration domain. In order to obtain a numerically stable result and to reduce the Monte Carlo integration error we use a multi-channel Monte Carlo method [16, 19], which is briefly outlined in the following.

Before turning to the multi-channel method, we consider the treatment of a single channel. We choose a suitable set $\vec{\Phi}$ of $3n-4$ phase-space variables to describe a point in phase space, and determine the corresponding physical region V and the relation $k_i(\vec{\Phi})$ between the phase-space variables $\vec{\Phi}$ and the momenta $k_1,\dots k_n$. The phase-space integration of (3.1) reads

$$I_n = \int\mathrm{d}\sigma = \int_V \mathrm{d}\vec{\Phi}\,\rho\Big(k_i(\vec{\Phi})\Big)\,f\Big(k_i(\vec{\Phi})\Big), \tag{3.2}$$

$$f\Big(k_i(\vec{\Phi})\Big) = \frac{(2\pi)^{4-3n}}{2s}\left|\mathcal{M}\left(p_+,p_-,k_1(\vec{\Phi}),\dots,k_n(\vec{\Phi})\right)\right|^2,$$

where ρ is the phase-space density. For the random generation of the events, we further transform the integration variables $\vec{\Phi}$ to $3n-4$ new variables $\vec{r} = (r_i)$ with a hypercube as integration domain: $\vec{\Phi} = \vec{h}(\vec{r})$ with $0 \le r_i \le 1$. We obtain

$$I_n = \int_V \mathrm{d}\vec{\Phi}\,\rho\Big(k_i(\vec{\Phi})\Big)\,f\Big(k_i(\vec{\Phi})\Big) = \int_0^1 \mathrm{d}\vec{r}\,\frac{f\Big(k_i(\vec{h}(\vec{r}))\Big)}{g\Big(k_i(\vec{h}(\vec{r}))\Big)}\,, \tag{3.3}$$

where g is the probability density of events generated in phase space, defined by

$$\frac{1}{g\Big(k_i(\vec{\Phi})\Big)} = \rho\Big(k_i(\vec{\Phi})\Big)\left|\frac{\partial\vec{h}(\vec{r})}{\partial\vec{r}}\right|_{\vec{r}=\vec{h}^{-1}(\vec{\Phi})}. \tag{3.4}$$

If f varies strongly, the efficiency of the Monte Carlo method can be considerably enhanced by choosing the mapping of random numbers $\vec{r}$ into $\vec{\Phi}$ in such a way that the resulting density g mimics the behaviour of $|f|$. For this *importance sampling*, the choice of $\vec{\Phi}$ is guided by the peaking structure of f, which is determined by the propagators in a characteristic Feynman diagram.

We choose the variables $\vec{\Phi}$ in such a way that the invariants corresponding to the propagators are included. Accordingly, we decompose the n-particle final state into $2 \to 2$

scattering processes with subsequent 1 → 2 decays. The variables $\vec{\Phi}$ consist of Lorentz invariants s_i, t_i, defined as the squares of time- and space-like momenta, respectively, and of polar and azimuthal angles θ_i, ϕ_i, defined in appropriate frames. A detailed description of the parameterization of an n-particle phase space in terms of invariants and angles can be found in Ref. [30]. The parameterization of the invariants s_i, t_i in $\vec{\Phi} = \vec{h}(\vec{r})$ is chosen in such a way that the propagator structure of the function f is compensated by a similar behaviour in the density g. More precisely, if f contains Breit–Wigner resonances or distributions like $s_i^{-\nu}$, which are relevant for massless propagators, appropriate parameterizations of s_i are given by:

- Breit–Wigner resonances:

$$\begin{aligned} s_i &= M_{\mathrm{V}}^2 + M_{\mathrm{V}}\Gamma_{\mathrm{V}} \tan[y_1 + (y_2 - y_1) r_i] \\ &\text{with } \; y_{1,2} = \arctan\left(\frac{s_{\min,\max} - M_{\mathrm{V}}^2}{M_{\mathrm{V}}\Gamma_{\mathrm{V}}}\right); \end{aligned} \tag{3.5}$$

- propagators of massless particles:

$$\begin{aligned} \nu \neq 1: \qquad s_i &= \left[s_{\max}^{1-\nu} r_i + s_{\min}^{1-\nu}(1 - r_i)\right]^{1/(1-\nu)}, \\ \nu = 1: \qquad s_i &= \exp\left[\ln(s_{\max}) r_i + \ln(s_{\min})(1 - r_i)\right]. \end{aligned} \tag{3.6}$$

The parameter ν can be tuned to optimize the Monte Carlo integration and should be chosen $\gtrsim 1$. The naive expectation $\nu = 2$ is not necessarily the best choice, because the propagator poles of the differential cross section are partly cancelled in the collinear limit. The remaining variables in $\vec{\Phi} = \vec{h}(\vec{r})$, i.e. those for which f is expected not to exhibit a peaking behaviour, are generated as follows:

$$s_i = s_{\max} r_i + s_{\min}(1 - r_i), \qquad \phi_i = 2\pi r_i, \qquad \cos\theta_i = 2r_i - 1. \tag{3.7}$$

The absolute values of the invariants t_i are generated in the same way as s_i. The resulting density g of events in phase space is obtained as the product of the corresponding Jacobians, as given in (3.4). In the appendix, we provide an explicit example for an event generation with a specific choice of mappings $k_i(\vec{\Phi})$ and $\vec{h}(\vec{r})$, and for the calculation of the corresponding density g.

The differential cross sections of the processes $\mathrm{e}^+\mathrm{e}^- \to 4f$ and especially $\mathrm{e}^+\mathrm{e}^- \to 4f\gamma$ possess very complex peaking structures so that the peaks in the integrand $f(\vec{\Phi})$ in (3.3) cannot be described properly by only one single density $g(\vec{\Phi})$. The *multi-channel approach* [16, 19] suggests a solution to this problem. For each peaking structure we choose a suitable set $\vec{\Phi}_k$, and accordingly a mapping of random numbers r_i into $\vec{\Phi}_k$: $\vec{\Phi}_k = \vec{h}_k(\vec{r})$ with $0 \leq r_i \leq 1$, so that the resulting density g_k describes this particular peaking behaviour of f. All densities g_k are combined into one density g_{tot} that is expected to smoothen the integrand over the whole phase-space integration region. The phase-space integral of (3.3) reads

$$I_n = \sum_{k=1}^{M} \int_V \mathrm{d}\vec{\Phi}_k \, \rho_k\Big(k_i(\vec{\Phi}_k)\Big) \, g_k\Big(k_i(\vec{\Phi}_k)\Big) \, \frac{f\Big(k_i(\vec{\Phi}_k)\Big)}{g_{\mathrm{tot}}\Big(k_i(\vec{\Phi}_k)\Big)} = \sum_{k=1}^{M} \int_0^1 \mathrm{d}\vec{r} \, \frac{f\Big(k_i(\vec{h}_k(\vec{r}))\Big)}{g_{\mathrm{tot}}\Big(k_i(\vec{h}_k(\vec{r}))\Big)}, \tag{3.8}$$

with

$$g_{\rm tot}\Big(k_i(\vec{\Phi}_k)\Big) = \sum_{l=1}^{M} g_l\Big(k_i(\vec{\Phi}_k)\Big), \qquad \frac{1}{g_l\Big(k_i(\vec{\Phi}_k)\Big)} = \rho_l\Big(k_i(\vec{\Phi}_k)\Big) \left|\frac{\partial \vec{h}_l(\vec{r})}{\partial \vec{r}}\right|_{\vec{r}=\vec{h}_k^{-1}(\vec{\Phi}_k)} . \tag{3.9}$$

The different mappings $\vec{h}_k(\vec{r})$ are called channels, and M is the number of all channels.

In order to reduce the Monte Carlo error further, we adopt the method of weight optimization of Ref. [20] and introduce *a-priori weights* $\alpha_k, k = 1, \dots, M$ ($\alpha_k \geq 0$ and $\sum_{k=1}^{M} \alpha_k = 1$). The channel k that is used to generate the event is picked randomly with probability α_k, i.e.

$$\begin{aligned} I_n &= \sum_{k=1}^{M} \alpha_k \int_V {\rm d}\vec{\Phi}_k\, \rho_k\Big(k_i(\vec{\Phi}_k)\Big) g_k\Big(k_i(\vec{\Phi}_k)\Big) \frac{f\Big(k_i(\vec{\Phi}_k)\Big)}{g_{\rm tot}\Big(k_i(\vec{\Phi}_k)\Big)} \\ &= \int_0^1 {\rm d}r_0 \sum_{k=1}^{M} \theta(r_0 - \beta_{k-1})\theta(\beta_k - r_0) \int_V {\rm d}\vec{\Phi}_k\, \rho_k\Big(k_i(\vec{\Phi}_k)\Big) g_k\Big(k_i(\vec{\Phi}_k)\Big) \frac{f\Big(k_i(\vec{\Phi}_k)\Big)}{g_{\rm tot}\Big(k_i(\vec{\Phi}_k)\Big)} \\ &= \int_0^1 {\rm d}r_0 \sum_{k=1}^{M} \theta(r_0 - \beta_{k-1})\theta(\beta_k - r_0) \int_0^1 {\rm d}\vec{r}\, \frac{f\Big(k_i(\vec{h}_k(\vec{r}))\Big)}{g_{\rm tot}\Big(k_i(\vec{h}_k(\vec{r}))\Big)}, \end{aligned} \tag{3.10}$$

where $\beta_0 = 0, \beta_j = \sum_{k=1}^{j} \alpha_k, j = 1, \dots, M-1$, $\beta_M = \sum_{k=1}^{M} \alpha_k = 1$, and

$$g_{\rm tot}\Big(k_i(\vec{\Phi}_k)\Big) = \sum_{l=1}^{M} \alpha_l g_l\Big(k_i(\vec{\Phi}_k)\Big), \tag{3.11}$$

is the total density of the event.

For the processes $e^+e^- \to 4f$ we have between 6 and 128 different channels, for $e^+e^- \to 4f\gamma$ between 14 and 928 channels. Each channel smoothens a particular combination of propagators that results from a characteristic Feynman diagram. We have written phase-space generators in a generic way for several classes of channels determined by the chosen set of invariants s_i, t_i. The channels within one class differ in the choice of the mappings (3.5), (3.6), and (3.7) and the order of the external particles. We did not include special channels for interference contributions.

The α_k-dependence of the quantity

$$W(\vec{\alpha}) = \frac{1}{N} \sum_{j=1}^{N} [w(r_0^j, \vec{r}^j)]^2, \tag{3.12}$$

where $w = f/g_{\rm tot}$ is the weight assigned to the Monte Carlo point $(r_0^j, \vec{r}^j)$ of the jth event, can be exploited to minimize the expected Monte Carlo error

$$\delta \bar{I}_n = \sqrt{\frac{W(\vec{\alpha}) - \bar{I}_n^2}{N}}, \tag{3.13}$$

with the Monte Carlo estimate of I_n

$$\bar{I}_n = \frac{1}{N} \sum_{j=1}^{N} w(r_0^j, \vec{r}^j) \tag{3.14}$$

by trying to choose an optimal set of a-priori weights. We perform the search for an optimal set of α_k by using an *adaptive optimization* method, as described in Ref. [20]. After a certain number of generated events a new set of a-priori weights α_k^{new} is calculated according to

$$\alpha_k^{\mathrm{new}} \propto \alpha_k \sqrt{\frac{1}{N} \sum_{j=1}^{N} \frac{g_k\Big(k_i(\vec{h}_k(\vec{r}^{\,j}))\Big)\,[w(r_0^j, \vec{r}^{\,j})]^2}{g_{\mathrm{tot}}\Big(k_i(\vec{h}_k(\vec{r}^{\,j}))\Big)}}, \qquad \sum_{k=1}^{M} \alpha_k^{\mathrm{new}} = 1. \tag{3.15}$$

Based on the above approach, we have written two independent Monte Carlo programs. While the general strategy is similar, the programs differ in the explicit phase-space generation.

4 Numerical results

If not stated otherwise we use the complex-mass scheme and the following parameters:

$$\begin{aligned} \alpha &= 1/128.89, & \alpha_s &= 0.12, \\ M_{\mathrm{W}} &= 80.26\,\mathrm{GeV}, & \Gamma_{\mathrm{W}} &= 2.05\,\mathrm{GeV}, \\ M_{\mathrm{Z}} &= 91.1884\,\mathrm{GeV}, & \Gamma_{\mathrm{Z}} &= 2.46\,\mathrm{GeV}. \end{aligned} \tag{4.1}$$

In the complex-mass scheme, the weak mixing angle is defined in (2.45), in all other schemes it is fixed by $c_{\mathrm{w}} = M_{\mathrm{W}}/M_{\mathrm{Z}}$, $s_{\mathrm{w}}^2 = 1 - c_{\mathrm{w}}^2$.

The energy in the centre-of-mass (CM) system of the incoming electron and positron is denoted by $\sqrt{s}$. Concerning the phase-space integration, we apply the canonical cuts of the ADLO/TH detector,

$$\begin{aligned} \theta(l,\mathrm{beam}) &> 10^\circ, & \theta(l,l') &> 5^\circ, & \theta(l,q) &> 5^\circ, \\ \theta(\gamma,\mathrm{beam}) &> 1^\circ, & \theta(\gamma,l) &> 5^\circ, & \theta(\gamma,q) &> 5^\circ, \\ E_\gamma &> 0.1\,\mathrm{GeV}, & E_l &> 1\,\mathrm{GeV}, & E_q &> 3\,\mathrm{GeV}, \\ m(q,q') &> 5\,\mathrm{GeV}, \end{aligned} \tag{4.2}$$

where $\theta(i,j)$ specifies the angle between the particles i and j in the CM system, and l, q, γ, and "beam" denote charged leptons, quarks, photons, and the beam electrons or positrons, respectively. The invariant mass of a quark pair qq' is denoted by $m(q,q')$. The cuts coincide with those defined in Ref. [23], except for the additional angular cut between charged leptons. The canonical cuts exclude all collinear and infrared singularities from phase space for all processes.

Although our helicity amplitudes and Monte Carlo programs allow for a treatment of arbitrary polarization configurations, we consider only unpolarized quantities in this paper.

All results are produced with 10^7 events. The calculation of the cross section for $\mathrm{e^+e^-} \to \mathrm{e^+e^-}\mu^+\mu^-$ requires about 50 minutes on a DEC ALPHA workstation with 500 MHz, the calculation of the cross section for $\mathrm{e^+e^-} \to \mathrm{e^+e^-}\mu^+\mu^-\gamma$ takes about 5 hours. The results of our two Monte Carlo programs agree very well. The numbers in parentheses in the following tables correspond to the statistical errors of the results of the Monte Carlo integrations.

4.1 Comparison with existing results

In order to compare our results for $\mathrm{e}^+\mathrm{e}^- \to 4f$ with Tables 6–8 of Ref. [31], we use the corresponding set of phase-space cuts and input parameters, i.e. the canonical cuts defined in (4.2), a CM energy of $\sqrt{s} = 190\,\mathrm{GeV}$, and the parameters $\alpha = \alpha(2M_\mathrm{W}) = 1/128.07$, $\alpha_s = 0.12$, $M_\mathrm{W} = 80.23\,\mathrm{GeV}$, $\Gamma_\mathrm{W} = 2.0337\,\mathrm{GeV}$, $M_\mathrm{Z} = 91.1888\,\mathrm{GeV}$, and $\Gamma_\mathrm{Z} = 2.4974\,\mathrm{GeV}$. The value of s_w, which enters the couplings, is calculated from $\alpha(2M_\mathrm{W})/(2s_\mathrm{w}^2) = G_\mu M_\mathrm{W}^2/(\pi\sqrt{2})$ with $G_\mu = 1.16639 \times 10^{-5}\,\mathrm{GeV}^{-2}$.

In Table 1, we list the integrated cross sections for various processes $\mathrm{e}^+\mathrm{e}^- \to 4f$ with running widths and constant widths, and for the corresponding processes $\mathrm{e}^+\mathrm{e}^- \to 4f\gamma$ with constant widths. For processes involving gluon-exchange diagrams we give the cross sections resulting from the purely electroweak diagrams and those including the gluon-exchange contributions. The latter results include also the interference terms between purely electroweak and gluon-exchange diagrams. In Table 1 we provide a complete list of processes for vanishing fermion masses. All processes $\mathrm{e}^+\mathrm{e}^- \to 4f(\gamma)$ not explicitly listed are equivalent to one of the given processes.

For NC processes $\mathrm{e}^+\mathrm{e}^- \to 4f$ with four neutrinos or four quarks in the final state we find small deviations of roughly 0.2% between the results with constant and running widths. Assuming that a running width has been used in Ref. [31], we find very good agreement.

Unfortunately we cannot compare with most of the publications [12, 13, 14, 15] for the bremsstrahlung processes $\mathrm{e}^+\mathrm{e}^- \to 4f\gamma$. In those papers, either the cuts are not (completely) specified, or collinear photon emission is not excluded, and the corresponding fermion-mass effects are taken into account. Note that the contributions of collinear photons dominate the results given there.

We have compared our results with the ones given in Refs. [10, 11], where the total cross sections for $\mathrm{e}^+\mathrm{e}^- \to 4f\gamma$ have been calculated for the purely leptonic and the semi-leptonic final states. As done in Refs. [10, 11] only diagrams involving two resonant W bosons have been taken into account for this comparison. Table 2 contains our results corresponding to Table 2 of Ref. [10]. Based on Refs. [10, 11], we have chosen $\sqrt{s} = 200\,\mathrm{GeV}$ and the input parameters $\alpha = 1/137.03599$, $M_\mathrm{W} = 80.9\,\mathrm{GeV}$, $\Gamma_\mathrm{W} = 2.14\,\mathrm{GeV}$, $M_\mathrm{Z} = 91.16\,\mathrm{GeV}$, $\Gamma_\mathrm{Z} = 2.46\,\mathrm{GeV}$, s_w obtained from $\alpha/(2s_\mathrm{w}^2) = G_\mu M_\mathrm{W}^2/(\pi\sqrt{2})$ with $G_\mu = 1.16637 \times 10^{-5}\,\mathrm{GeV}^{-2}$, and constant gauge-boson widths. The energy of the photon is required to be larger than $E_{\gamma,\mathrm{min}}$, and the angle between the photon and any charged fermion must be larger than $\theta_{\gamma,\mathrm{min}}$. A maximal photon energy is required, $E_\gamma < 60\,\mathrm{GeV}$, in order to exclude contributions from the Z resonance. Our results are consistent with those of Refs. [10, 11] within the statistical error of 1% given there. In some cases we find deviations of 2%.[2]

4.2 Comparison of finite-width schemes

As discussed in Refs. [26, 29], particular care has to be taken when implementing the finite gauge-boson widths. Differences between results obtained with running or constant widths can already be seen in Table 1, where a typical LEP2 energy is considered. In

---

[2] Note that the input specified in Refs. [10, 11] is not completely clear even if the information of both publications is combined.

$\sigma/\,\mathrm{fb}$	$\mathrm{e^+e^-} \to 4f$ running width	$\mathrm{e^+e^-} \to 4f$ constant width	$\mathrm{e^+e^-} \to 4f\gamma$ constant width
$\nu_\mathrm{e}\bar\nu_\mathrm{e}\mathrm{e^-e^+}$	256.7(3)	257.1(7)	89.4(2)
$\nu_\mu\mu^+\mathrm{e}^-\bar\nu_\mathrm{e}$	227.4(1)	227.5(1)	79.1(1)
$\nu_\mu\bar\nu_\mu\mu^-\mu^+$	228.7(1)	228.8(1)	81.0(2)
$\nu_\mu\mu^+\tau^-\bar\nu_\tau$	218.55(9)	218.57(9)	76.7(1)
$\mathrm{e^-e^+e^-e^+}$	109.1(3)	109.4(3)	38.8(4)
$\mathrm{e^-e^+}\mu^-\mu^+$	116.6(3)	116.4(3)	43.4(4)
$\mu^-\mu^+\mu^-\mu^+$	5.478(5)	5.478(5)	3.37(1)
$\mu^-\mu^+\tau^-\tau^+$	11.02(1)	11.02(1)	6.78(3)
$\mathrm{e^-e^+}\nu_\mu\bar\nu_\mu$	14.174(9)	14.150(9)	5.36(1)
$\nu_\mathrm{e}\bar\nu_\mathrm{e}\mu^-\mu^+$	17.78(6)	17.73(6)	6.63(2)
$\nu_\tau\bar\nu_\tau\mu^-\mu^+$	10.108(8)	10.103(8)	4.259(9)
$\nu_\mathrm{e}\bar\nu_\mathrm{e}\nu_\mathrm{e}\bar\nu_\mathrm{e}$	4.089(1)	4.082(1)	0.7278(7)
$\nu_\mathrm{e}\bar\nu_\mathrm{e}\nu_\mu\bar\nu_\mu$	8.354(2)	8.337(2)	1.512(1)
$\nu_\mu\bar\nu_\mu\nu_\mu\bar\nu_\mu$	4.069(1)	4.057(1)	0.7434(7)
$\nu_\mu\bar\nu_\mu\nu_\tau\bar\nu_\tau$	8.241(2)	8.218(2)	1.511(1)
$\mathrm{u\,\bar d\,e^-}\bar\nu_\mathrm{e}$	693.5(3)	693.6(3)	220.8(4)
$\mathrm{u\,\bar d}\,\mu^-\bar\nu_\mu$	666.7(3)	666.7(3)	214.5(4)
$\mathrm{e^-e^+u\,\bar u}$	86.87(9)	86.82(9)	32.3(2)
$\mathrm{e^-e^+d\,\bar d}$	43.02(4)	42.95(4)	16.17(8)
$\mathrm{u\,\bar u}\,\mu^-\mu^+$	24.69(2)	24.69(2)	12.70(4)
$\mathrm{d\,\bar d}\,\mu^-\mu^+$	23.73(1)	23.73(1)	10.43(2)
$\nu_\mathrm{e}\bar\nu_\mathrm{e}\mathrm{u\,\bar u}$	24.00(2)	23.95(2)	6.84(1)
$\nu_\mathrm{e}\bar\nu_\mathrm{e}\mathrm{d\,\bar d}$	20.657(8)	20.62(1)	4.319(6)
$\mathrm{u\,\bar u}\,\nu_\mu\bar\nu_\mu$	21.080(5)	21.050(5)	6.018(9)
$\mathrm{d\,\bar d}\,\nu_\mu\bar\nu_\mu$	19.863(5)	19.817(5)	4.156(5)
$\mathrm{u\,\bar u\,d\,\bar d}$	2064.1(9), 2140.8(9)	2064.3(9), 2141(1)	615(1), 672(1)
$\mathrm{u\,\bar d\,s\,\bar c}$	2015.2(8)	2015.3(8)	598(1)
$\mathrm{u\,\bar u\,u\,\bar u}$	25.738(7), 71.28(4)	25.721(7), 71.30(4)	9.78(2), 42.1(1)
$\mathrm{d\,\bar d\,d\,\bar d}$	23.494(6), 51.35(3)	23.448(6), 51.32(3)	5.527(7), 28.68(4)
$\mathrm{u\,\bar u\,c\,\bar c}$	51.61(1), 144.72(9)	51.57(1), 144.75(9)	19.61(4), 86.1(2)
$\mathrm{u\,\bar u\,s\,\bar s}$	49.68(1), 126.52(8)	49.62(1), 126.52(8)	15.17(2), 75.1(2)
$\mathrm{d\,\bar d\,s\,\bar s}$	47.13(1), 104.79(6)	47.02(1), 104.74(6)	11.10(2), 59.2(1)

Table 1: Integrated cross sections for all representative processes $\mathrm{e^+e^-} \to 4f$ with running widths and constant widths and for the corresponding processes $\mathrm{e^+e^-} \to 4f\gamma$ with constant widths. If two numbers are given, the first results from pure electroweak diagrams and the second involves in addition gluon-exchange contributions.

$E_{\gamma,\mathrm{min}} =$		1 GeV	5 GeV	10 GeV	15 GeV
	$\theta_{\gamma,\mathrm{min}}$	σ/fb			
leptonic process	1°	53.54(8)	27.57(3)	16.96(2)	11.22(2)
	5°	32.65(4)	16.98(3)	10.48(2)	6.94(1)
	10°	23.48(3)	12.30(2)	7.61(2)	5.04(1)
	15°	18.03(2)	9.51(2)	5.90(1)	3.90(1)
semi-leptonic process	1°	141.9(2)	71.90(8)	43.56(5)	28.26(4)
	5°	86.8(1)	44.25(6)	26.78(4)	17.40(3)
	10°	62.29(7)	31.92(5)	19.40(4)	12.61(3)
	15°	47.42(5)	24.50(4)	14.97(3)	9.77(2)

Table 2: Comparison with Table 2 of Ref. [10]: Cross sections resulting from diagrams involving two resonant W bosons for purely leptonic and semi-leptonic final states and several photon separation cuts

σ/ fb	$\sqrt{s} =$	189 GeV	500 GeV	2 TeV	10 TeV
$\mathrm{e}^+\mathrm{e}^- \to \mathrm{u}\,\bar{\mathrm{d}}\,\mu^-\bar{\nu}_\mu$	constant width	703.5(3)	237.4(1)	13.99(2)	0.624(3)
	running width	703.4(3)	238.9(1)	34.39(3)	498.8(1)
	complex-mass scheme	703.1(3)	237.3(1)	13.98(2)	0.624(3)
$\mathrm{e}^+\mathrm{e}^- \to \mathrm{u}\,\bar{\mathrm{d}}\,\mu^-\bar{\nu}_\mu\,\gamma$	constant width	224.0(4)	83.4(3)	6.98(5)	0.457(6)
	running width	224.6(4)	84.2(3)	19.2(1)	368(6)
	complex-mass scheme	223.9(4)	83.3(3)	6.98(5)	0.460(6)
$\mathrm{e}^+\mathrm{e}^- \to \mathrm{u}\,\bar{\mathrm{d}}\,\mathrm{e}^-\bar{\nu}_\mathrm{e}$	constant width	730.2(3)	395.3(2)	211.0(2)	32.38(6)
	running width	729.8(3)	396.9(2)	231.5(2)	530.2(6)
	complex-mass scheme	729.8(3)	395.1(2)	210.9(2)	32.37(6)
$\mathrm{e}^+\mathrm{e}^- \to \mathrm{u}\,\bar{\mathrm{d}}\,\mathrm{e}^-\bar{\nu}_\mathrm{e}\,\gamma$	constant width	230.0(4)	136.5(5)	84.0(7)	16.8(5)
	running width	230.6(4)	137.3(5)	95.7(7)	379(6)
	complex-mass scheme	229.9(4)	136.4(5)	84.1(6)	16.8(5)

Table 3: Comparison of different width schemes for several processes and energies

$\sqrt{s}$/ GeV	189				500			
V_1V_2	WW	ZZ	γZ	$\gamma\gamma$	WW	ZZ	γZ	$\gamma\gamma$
$E_\gamma^{V_1V_2}$/ GeV	26.3	6.5	72.5	94.5	224	217	242	250

Table 4: Photon energies $E_\gamma^{V_1V_2}$ corresponding to thresholds

Table 3 we compare predictions for integrated cross sections obtained by using a constant width, a running width, or the complex-mass scheme for several energies. We consider two semi-leptonic final states for $\mathrm{e^+e^-} \to 4f(\gamma)$. The numbers show that the constant width and the complex-mass scheme yield the same results within the statistical accuracy for $\mathrm{e^+e^-} \to 4f$ and $\mathrm{e^+e^-} \to 4f\gamma$. In contrast, the results with the running width produce totally wrong results for high energies. The difference of the running width with respect to the other implementations of the finite width is up to 1% already for 500 GeV. Thus, the running width should not be used for linear-collider energies. As already stated above, our default treatment of the finite width is the complex-mass scheme in the following.

4.3 Survey of photon-energy spectra

In Figure 2 we show the photon-energy spectra of several processes for the typical LEP2 energy of 189 GeV and a possible linear-collider energy of 500 GeV. The upper plots contain CC and CC/NC processes, the plots in the middle and the lower plots contain NC processes. Several spectra show threshold or peaking structures. These structures are caused by diagrams in which the photon is emitted from the initial state. The two important classes of diagrams are shown in Figure 3.

The first class, shown in Figure 3a, corresponds to triple-gauge-boson-production subprocesses which yield dominant contributions as long as the two virtual gauge bosons V_1 and V_2 can become simultaneously resonant. If the real photon takes the energy E_γ, defined in the CM system, only the energy $\sqrt{s'}$, with

$$s' = s - 2\sqrt{s}\,E_\gamma, \tag{4.3}$$

is available for the production of the gauge-boson pair V_1V_2. If at least one of the gauge bosons is massive, and if the photon becomes too hard, the two gauge bosons cannot be produced on shell anymore, so that the spectrum falls off for E_γ above the corresponding threshold $E_\gamma^{V_1V_2}$. Using the threshold condition for the on-shell production of the V_1V_2 pair,

$$\sqrt{s'} > M_{V_1} + M_{V_2}, \tag{4.4}$$

the value of $E_\gamma^{V_1V_2}$ is determined by

$$E_\gamma^{V_1V_2} = \frac{s - (M_{V_1} + M_{V_2})^2}{2\sqrt{s}}. \tag{4.5}$$

The values of the photon energies that cause such thresholds can be found in Table 4. The value $E_\gamma^{\gamma\gamma}$ corresponds to the upper endpoint of the photon-energy spectrum, which is given by the beam energy $\sqrt{s}/2$. Since $\sqrt{s'}$ is fully determined by s and E_γ, the

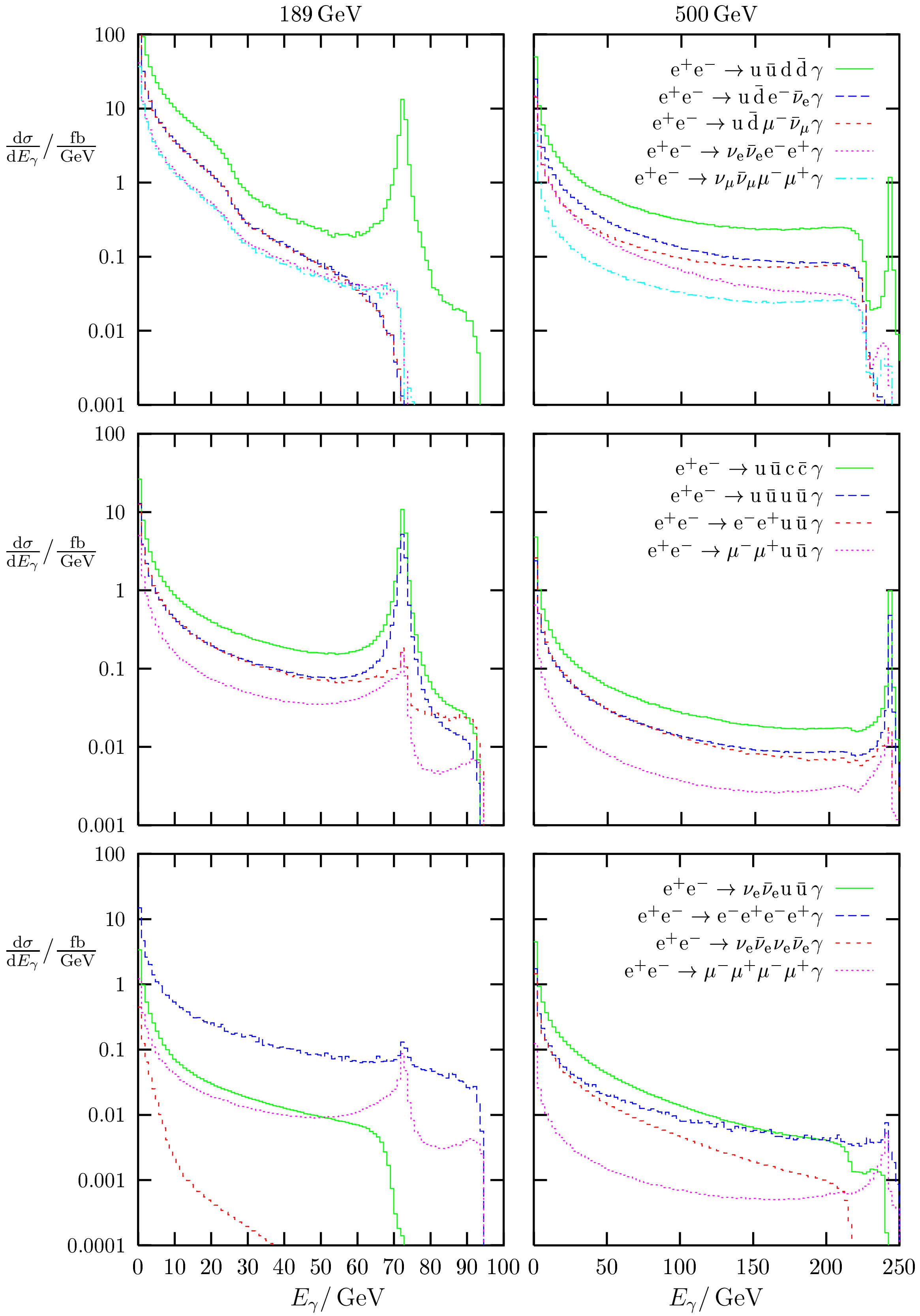

Figure 2: Photon-energy spectra for several processes and for $\sqrt{s} = 189\,\text{GeV}$ and $500\,\text{GeV}$

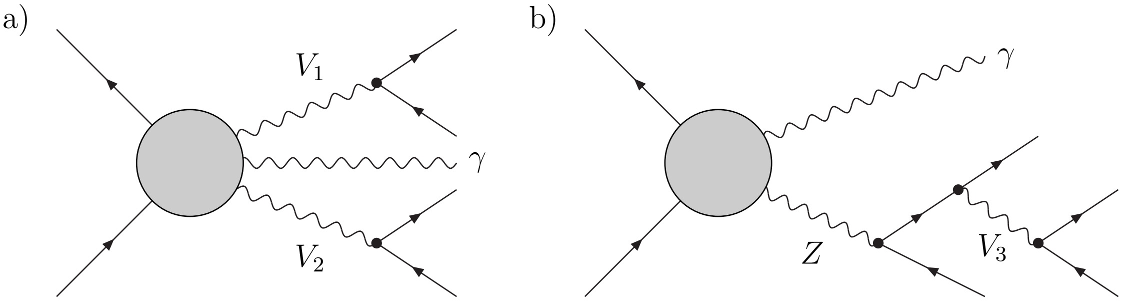

Figure 3: Diagrams for important subprocesses, where $V_1, V_2 = \mathrm{W}, \mathrm{Z}, \gamma$, and $V_3 = \gamma, \mathrm{g}$

contribution of the V_1V_2-production subprocess to the E_γ spectrum qualitatively follows the energy dependence of the total cross section for V_1V_2 production (cf. Ref. [31], Fig. 1) above the corresponding thresholds. The cross sections for $\gamma\gamma$ and γZ production strongly increase with decreasing energy, while the ones for ZZ and WW production are comparably flat. Thus, the $\gamma\gamma$ and γZ-production subprocesses introduce contributions in the photon-energy spectra with resonance-like structures, whereas the ones with ZZ or WW pairs yield edges.

The second class of important diagrams, shown in Figure 3b corresponds to the production of a photon and a resonant Z boson that decays into four fermions. These diagrams are important if the gauge boson V_3 is also resonant, i.e. a photon or a gluon with small invariant mass. In this case, the kinematics fixes the energy of the real photon to

$$E_\gamma = E_\gamma^{\gamma\mathrm{Z}} = \frac{s - M_\mathrm{Z}^2}{2\sqrt{s}}, \tag{4.6}$$

which corresponds to the γZ threshold in Table 4. This subprocess gives rise to resonance structures at $E_\gamma^{\gamma\mathrm{Z}}$, which are even enhanced by α_s/α in the presence of gluon exchange.

In the photon-energy spectra of Figure 2 all these threshold and resonance effects are visible. The effect of the γZ peak can be nicely seen in different photon-energy spectra, in particular in those where gluon-exchange diagrams contribute (cf. also Figure 5). The effect of the WW threshold is present in the upper two plots of Figure 2. In the plot for $\sqrt{s} = 189\,\mathrm{GeV}$ the threshold for single W production causes the steep drop of the spectrum for the pure CC processes above $70\,\mathrm{GeV}$. Note that the CC cross sections are an order of magnitude larger than the NC cross sections if the WW channel is open. The ZZ threshold is visible in the middle and lower plots for $\sqrt{s} = 500\,\mathrm{GeV}$. The γZ threshold (resulting from the graphs of Figure 3a) is superimposed on the γZ peak (resulting from the graphs of Figure 3b) and therefore best recognizable in those channels where the γZ peak is absent or suppressed, i.e. where a neutrino pair is present in the final state or where at least no gluon-exchange diagrams contribute. Processes with four neutrinos in the final state do not involve photonic diagrams and are therefore small above the ZZ threshold. The effects of the triple-photon-production subprocess appear as a tendency of some photon-energy spectra to increase near the maximal value of E_γ for two charged fermion–antifermion pairs in the final state.

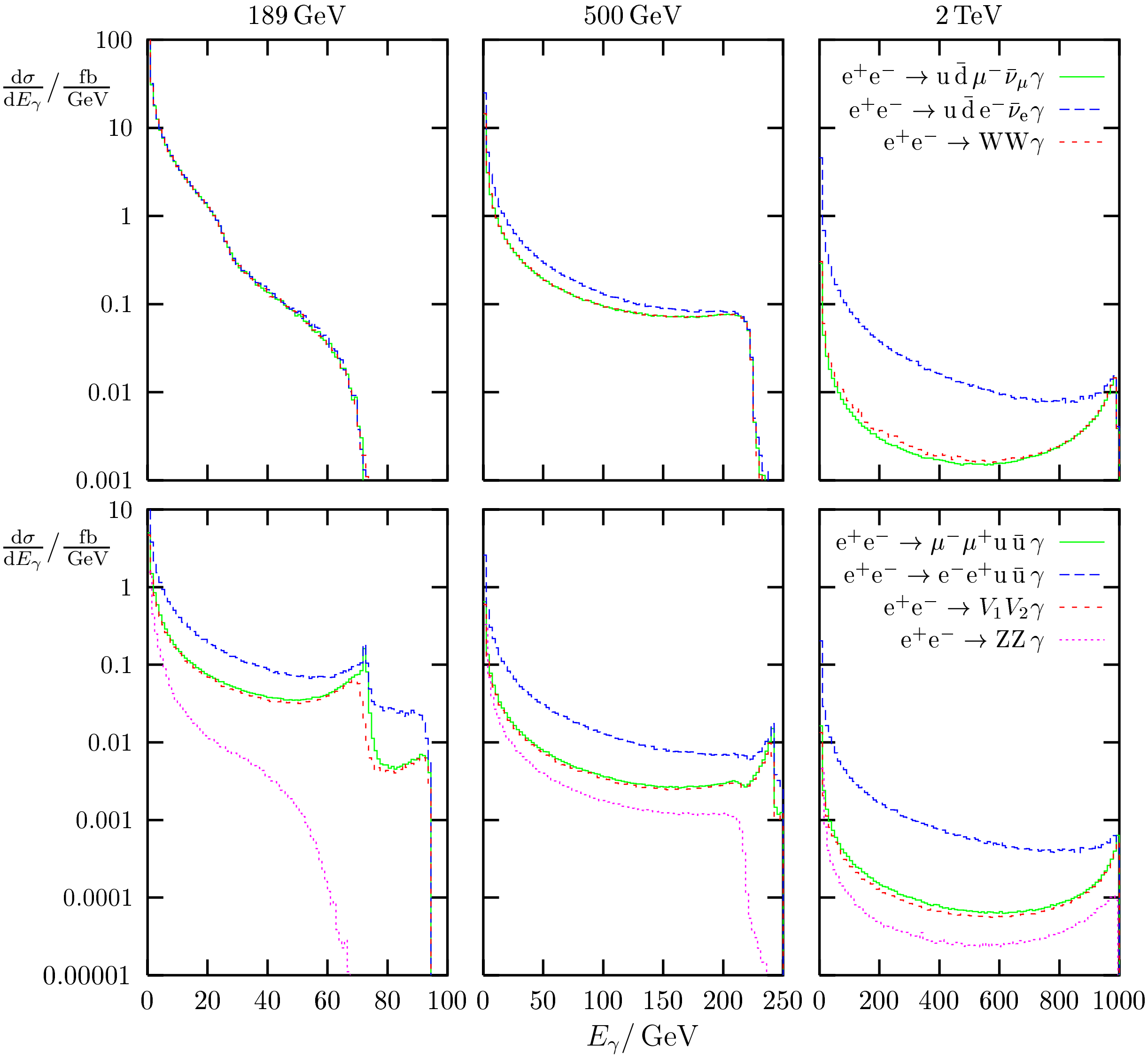

Figure 4: Photon-energy spectra resulting from the triple-gauge-boson-production subprocesses compared to those resulting from all diagrams (V_1V_2 includes ZZ, γZ, and $\gamma\gamma$)

4.4 Triple-gauge-boson-production subprocesses

In Figure 4 we compare predictions that are based on the full set of diagrams with those that include only the graphs associated with the triple-gauge-boson-production subprocesses, i.e. the graphs in Figure 3a. In addition we consider the contributions of the ZZγ-production subprocess alone. For CC processes, the photon-energy spectra resulting from the $W^+W^-\gamma$-production subprocess are close to those resulting from all diagrams at LEP2 energies, but large differences are found for higher energies and $e^\pm$ in the final state. Note that the spectra are shown on a logarithmic scale. Even at LEP2 energies the differences between the predictions for different final states may be important, as can be seen, for instance, in Table 1 by comparing the cross sections of $e^+e^- \to u\,\bar{d}\,\mu^-\bar{\nu}_\mu\gamma$ and $e^+e^- \to u\,\bar{d}\,e^-\bar{\nu}_e\gamma$. In the case of NC processes, already for 189 GeV the contributions from ZZγ, Z$\gamma\gamma$, and $\gamma\gamma\gamma$ production are not sufficient: in the vicinity of the γZ peak sizeable contributions result from the γZ-production subprocess

$\sigma/\,\mathrm{fb}$	ew and gluon	purely ew	gluon	interference
$\mathrm{e^+e^-\to u\,\bar{u}\,c\,\bar{c}}$	52.98(4)	21.560(6)	31.38(3)	0.04(5)
$\mathrm{e^+e^-\to u\,\bar{u}\,c\,\bar{c}}\,\gamma$	29.8(1)	10.38(4)	19.6(1)	−0.1(1)
$\mathrm{e^+e^-\to u\,\bar{u}\,u\,\bar{u}}$	26.25(2)	10.765(3)	15.34(1)	0.14(2)
$\mathrm{e^+e^-\to u\,\bar{u}\,u\,\bar{u}}\,\gamma$	14.83(7)	5.16(2)	9.52(5)	0.15(9)
$\mathrm{e^+e^-\to d\,\bar{d}\,u\,\bar{u}}$	901.2(6)	876.4(5)	24.24(2)	0.6(8)
$\mathrm{e^+e^-\to d\,\bar{d}\,u\,\bar{u}}\,\gamma$	290(1)	275(1)	14.82(8)	0(1)

Table 5: Full lowest order cross section (ew and gluon) and contributions of purely electroweak diagrams (ew), of gluon-exchange diagrams (gluon), and their interference for 500 GeV

(Figure 3b) even for the $\mu^+\mu^-\mathrm{u\,\bar{u}}\,\gamma$ final state. For $\mathrm{e^+e^-\to e^-e^+u\,\bar{u}}\,\gamma$ other diagrams become dominating everywhere. The contribution of $\mathrm{ZZ}\gamma$ production is always small and could only be enhanced by invariant-mass cuts. Note that the triple-gauge-boson-production diagrams form a gauge-invariant subset for NC processes, while this is not the case for CC processes.

4.5 Relevance of gluon-exchange contributions

In the analytical calculation of the matrix elements for $\mathrm{e^+e^-}\to 4f(\gamma)$ in Section 2 we have seen that NC processes with four quarks in the final state involve, besides purely electroweak, also gluon-exchange diagrams. Table 5 illustrates the impact of these diagrams on the integrated cross sections for a CM energy of 500 GeV. The results for the interference are obtained by subtracting the purely electroweak and the gluon contribution from the total cross section. For pure NC processes the contributions of gluon-exchange diagrams dominate over the purely electroweak graphs. This can be understood from the fact that the gluon-exchange diagrams are enhanced by the strong coupling constant, and, as discussed in Section 4.3, that the diagrams with gluons replaced by photons yield a sizeable contribution to the cross section. For the mixed CC/NC processes the purely electroweak diagrams dominate the cross section. Here, the contributions from the $\mathrm{W^+W^-}\gamma$-production subprocess are large compared to all other diagrams, even if the latter are enhanced by the strong coupling. At 500 GeV the gluon-exchange diagrams contribute to the cross section at the level of several per cent. The interference contributions are relatively small. As discussed at the end of Section 2.3.2, this is due to the fact that interfering electroweak and gluon-exchange diagrams involve different resonances. Note that the interference vanishes for $\mathrm{e^+e^-\to u\,\bar{u}\,c\,\bar{c}}\,\gamma$, and the corresponding numbers in Table 5 are only due to the Monte Carlo integration error.

In Figure 5 we show the photon-energy spectra for the processes $\mathrm{e^+e^-\to u\,\bar{u}\,d\,\bar{d}}\,\gamma$ and $\mathrm{e^+e^-\to u\,\bar{u}\,u\,\bar{u}}\,\gamma$ together with the separate contributions from purely electroweak and gluon-exchange diagrams. The pure electroweak contributions are similar to the ones for $\mathrm{e^+e^-\to u\,\bar{d}}\,\mu^-\bar{\nu}_\mu\,\gamma$ and $\mathrm{e^+e^-\to e^-e^+u\,\bar{u}}\,\gamma$ in Figure 2. For the NC process $\mathrm{e^+e^-\to u\,\bar{u}\,u\,\bar{u}}\,\gamma$, the photon-energy spectrum is dominated by the gluon-exchange contribution,

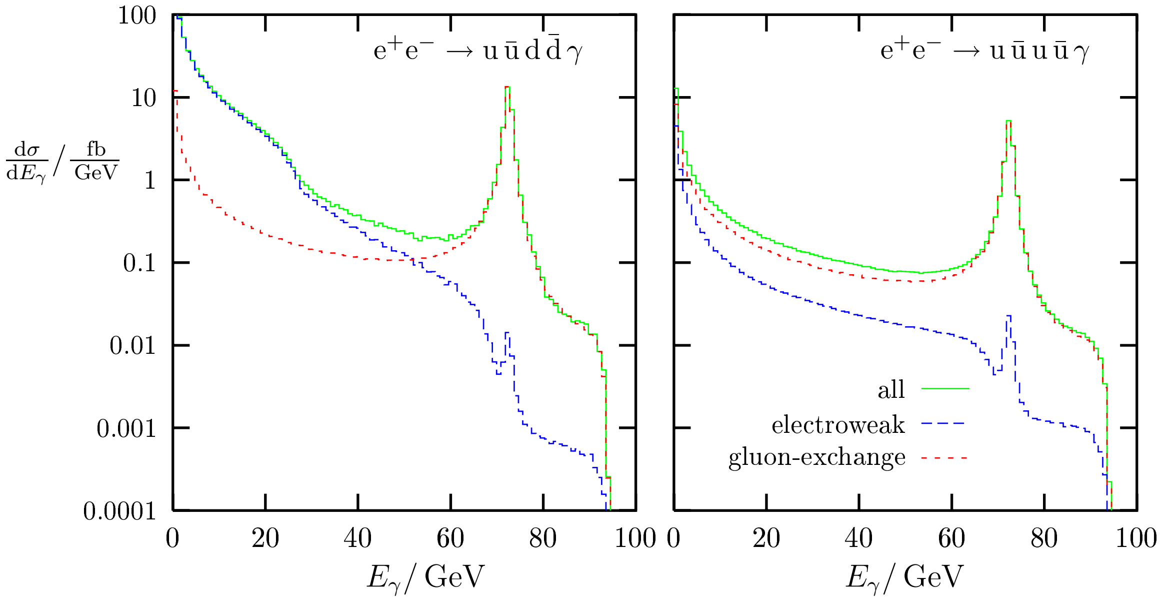

Figure 5: Electroweak and gluon-exchange contributions to the photon-energy spectra for $e^+e^- \to u\,\bar{u}\,d\,\bar{d}\,\gamma$ and $e^+e^- \to u\,\bar{u}\,u\,\bar{u}\,\gamma$ at $\sqrt{s} = 189\,\mathrm{GeV}$

which shows a strong peak at 72.5 GeV owing to the γZ-production subprocess. For the CC/NC process $e^+e^- \to u\,\bar{u}\,d\,\bar{d}\,\gamma$, the electroweak diagrams dominate below the WW threshold, whereas the gluon-exchange diagrams dominate at the γZ peak and above. The interference between purely electroweak and gluon-exchange diagrams is generally small.

5 Summary and outlook

The class of processes $e^+e^- \to 4\,\mathrm{fermions} + \gamma$ has been discussed in detail. After classifying the different final states according to their production mechanism, the sets of all Feynman graphs are reduced to two generic subsets that are related to the two basic graphs of the non-radiative processes $e^+e^- \to 4\,\mathrm{fermions}$. In this way, all helicity matrix elements are expressed in terms of two generic functions. Using the Weyl–van der Waerden spinor formalism, we have given compact expressions for these functions. We wrote two independent Monte Carlo programs, both using the multi-channel integration technique and an adaptive weight optimization procedure to reduce the Monte Carlo error. The results obtained with the two Monte Carlo programs agree well within the integration error.

The detailed discussion of numerical results comprises a survey of integrated cross sections and photon-energy spectra for all different final states. Moreover, we have numerically compared different ways to introduce finite decay widths of the massive gauge bosons. Similar to the known results for $e^+e^- \to 4\,\mathrm{fermions}$, we find that the application of running gauge-boson widths leads to totally wrong results for the radiative processes. Using constant widths consistently, leads to meaningful predictions. For the considered observables, the results for constant widths practically coincide with those obtained in a

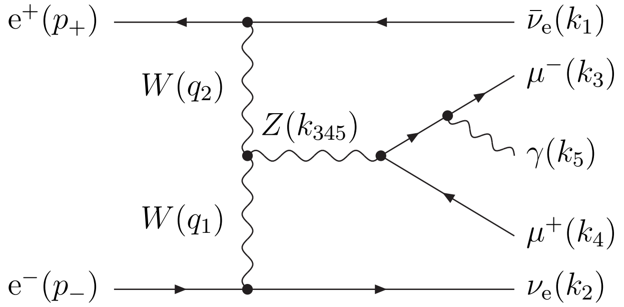

Figure 6: An example for a multi-peripheral diagram contributing to the process $\mathrm{e}^+\mathrm{e}^- \to \nu_\mathrm{e}\bar\nu_\mathrm{e}\mu^-\mu^+\gamma$

complex-mass scheme that fully respects gauge invariance. In the latter scheme gauge-boson masses are treated as complex parameters everywhere, in particular, leading to complex couplings. Similar to the situation for the well-known non-radiative processes, we find that for precise predictions the diagrams corresponding to triple-gauge-boson-production subprocesses are not sufficient and the inclusion of the other graphs is mandatory. Finally, we have investigated the relevance of gluon-exchange contributions. In general, both the purely electroweak contributions and the gluon-exchange contributions are relevant and either one can be dominant depending on the process and the considered observable. The interference of both contributions is at most at the per-cent level.

In this paper, we have assumed that the radiated photon appears as a detectable particle in the final state, i.e. soft and collinear photons are excluded by cuts. The inclusion of soft and collinear photons is, however, necessary if $\mathrm{e}^+\mathrm{e}^- \to 4\,\mathrm{fermions} + \gamma$ is considered as a correction to four-fermion production. The analytical results of this paper and the constructed Monte Carlo programs will be used as a building block in the evaluation of four-fermion production in $\mathrm{e}^+\mathrm{e}^-$ collisions including $\mathcal{O}(\alpha)$ corrections.

Appendix

An example for phase-space generation

To illustrate the phase-space generation in one channel, we choose the multi-peripheral diagram, shown in Figure 6. We determine the momentum configuration k_i from the phase-space variables s_i, t_i, ϕ_i, and θ_i with a suitable choice of mappings and calculate the resulting probability density g.

First we study the propagator structure of the Feynman diagram of Figure 6 and choose a set $\vec\Phi$ of 11 phase-space variables that is suitable for importance sampling. Our choice of $\vec\Phi$ consists of three time-like invariants

$$\begin{aligned} s_{35} &= k_{35}^2 = (k_3+k_5)^2, \\ s_{345} &= k_{345}^2 = (k_3+k_4+k_5)^2, \\ s_{1345} &= k_{1345}^2 = (k_1+k_3+k_4+k_5)^2, \end{aligned} \tag{A.1}$$

two space-like invariants

$$\begin{aligned} t_1 &= q_1^2 = (p_- - k_2)^2, \\ t_2 &= q_2^2 = (p_+ - k_1)^2, \end{aligned} \tag{A.2}$$

and six azimuthal and polar angles $\phi_{1,2,3,4}$ and $\theta_{3,4}$, respectively. As worked out in detail in Ref. [30], the 11-dimensional phase-space integral in (3.1) can be written as follows:

$$\begin{aligned} R_5(s) &= \int \left[\prod_{i=1}^{5} \mathrm{d}^4 k_i \, \delta\left(k_i^2\right) \theta(k_i^0)\right] \delta^{(4)}\left(p_+ + p_- - \sum_{i=1}^{5} k_i\right) \\ &= \int_V \mathrm{d}s_{35}\, \mathrm{d}s_{345}\, \mathrm{d}s_{1345}\, R_2(s)\, R_2(s_{1345})\, R_2(s_{345})\, R_2(s_{35}), \end{aligned} \tag{A.3}$$

where $\sqrt{s}$ denotes the CM energy with $s = (p_- + p_+)^2$. The phase space of the 2 → 5 scattering process is composed of the phase spaces of two 2 → 2 scattering processes with two subsequent 1 → 2 decays described by the following functions:

$R_2(s)$: First, we consider the 2 → 2 scattering process $p_+ + p_- \to k_{1345} + k_2$ in the system $\vec{p}_+ + \vec{p}_- = \vec{0}$ where the direction of $\vec{p}_+$ is chosen to be the positive z axis.

$R_2(s_{1345})$: Then, we boost and rotate to the system $\vec{k}'_{1345} = \vec{0}$ and describe the 2 → 2 scattering process $p'_+ + q'_1 \to k'_{345} + k'_1$, where the direction of $\vec{p'}_+$ is chosen to be the positive z axis.

$R_2(s_{345})$: Next, we define the 1 → 2 decay of the Z boson $k''_{345} \to k''_{35} + k''_4$ in its rest frame $\vec{k}''_{345} = \vec{0}$.

$R_2(s_{35})$: Finally, we treat the subsequent 1 → 2 decay of the virtual muon $k'''_{35} \to k'''_3 + k'''_5$ in its rest frame $\vec{k}'''_{35} = \vec{0}$.

For massless external fermions, $R_5(s)$ explicitly reads[3]

$$\begin{aligned} R_5(s) = &\int_{s_{35,\mathrm{cut}}}^{s} \mathrm{d}s_{35} \int_{s_{35}}^{s} \mathrm{d}s_{345} \int_{s_{345}}^{s} \mathrm{d}s_{1345} \left[\frac{1}{4s} \int_{t_{1,\min}}^{t_{1,\max}} \mathrm{d}t_1 \int_0^{2\pi} \mathrm{d}\phi_1\right] \\ &\times \left[\frac{1}{4\lambda^{1/2}(s_{1345}, t_1, 0)} \int_{t_{2,\min}}^{t_{2,\max}} \mathrm{d}t_2 \int_0^{2\pi} \mathrm{d}\phi_2\right] \\ &\times \left[\frac{\lambda^{1/2}(s_{345}, s_{35}, 0)}{8 s_{345}} \int_{-1}^{1} \mathrm{d}\cos\theta_3 \int_0^{2\pi} \mathrm{d}\phi_3\right] \left[\frac{1}{8} \int_{-1}^{1} \mathrm{d}\cos\theta_4 \int_0^{2\pi} \mathrm{d}\phi_4\right] \end{aligned} \tag{A.4}$$

with the kinematical function

$$\lambda(x, y, z) = x^2 + y^2 + z^2 - 2xy - 2yz - 2zx. \tag{A.5}$$

The limits on $t_{1,2}$ are the physical boundaries of the 2 → 2 scattering processes

$$\begin{aligned} t_{1,\min} &= s_{1345} - s, & t_{1,\max} &= 0, \\ t_{2,\min} &= (t_1 - s_{1345})(s_{1345} - s_{345})/s_{1345}, & t_{2,\max} &= 0. \end{aligned}$$

---

[3] As usual we set $f = 0$ outside the imposed cuts. However, to improve the efficiency of the phase-space generation, cuts can be included already in the physical boundaries of phase space. In our example we have introduced a lower cut on s_{35}.

In our example, we only have to cope with massive space-like propagators, so that we generate the invariants s_{35} and s_{345} according to (3.5) and (3.6), but do not apply importance sampling in the variables s_{1345}, $t_{1,2}$, $\phi_{1,2,3,4}$, and $\cos\theta_{3,4}$, which are generated according to (3.7). The resulting density g of (3.9) for this specific channel reads for $\nu \neq 1$,

$$\begin{aligned}\frac{1}{g} = {} & \frac{\lambda^{1/2}(s_{345}, s_{35}, 0)}{4^2\, 8^2\, s\, s_{345}\, \lambda^{1/2}(s_{1345}, t_1, 0)} \\ & \times s_{35}^{\nu}\, \frac{s^{1-\nu} - s_{35,\mathrm{cut}}^{1-\nu}}{1-\nu}\, \frac{[(s_{345} - M_{\mathrm{Z}}^2)^2 + M_{\mathrm{Z}}^2\Gamma_{\mathrm{Z}}^2]}{M_{\mathrm{Z}}\Gamma_{\mathrm{Z}}}\, (y_2 - y_1) \\ & \times (s - s_{345})\, |t_{1,\mathrm{min}}|\, |t_{2,\mathrm{min}}|\, 4\, (2\pi)^4 \end{aligned} \tag{A.6}$$

with $y_{1,2} = \arctan[(s_{1,2} - M_{\mathrm{Z}}^2)/(M_{\mathrm{Z}}\Gamma_{\mathrm{Z}})]$, $s_1 = s_{35}$, and $s_2 = s$. Finally, the event characterized by the four-momentum configuration $k_i, i = 1, \ldots, 5$, and the beam momenta are defined in terms of the generated invariants and angles as follows:

$$\begin{aligned} p_+^{\mu} &= \frac{\sqrt{s}}{2}(1, 0, 0, 1), \\ p_-^{\mu} &= \frac{\sqrt{s}}{2}(1, 0, 0, -1), \\ k_2^{\mu} &= \frac{\lambda^{1/2}(s, s_{1345}, 0)}{2\sqrt{s}}(1, -\cos\phi_1 \sin\theta_1, -\sin\phi_1 \sin\theta_1, -\cos\theta_1) \end{aligned} \tag{A.7}$$

with $\cos\theta_1 = (t_1 + 2p_-^0 k_2^0)/(2p_-^0 k_2^0)$,

$$k_1'^{\mu} = \frac{\lambda^{1/2}(s_{1345}, s_{345}, 0)}{2\sqrt{s_{1345}}}(1, \cos\phi_2 \sin\theta_2, \sin\phi_2 \sin\theta_2, \cos\theta_2) \tag{A.8}$$

with $\cos\theta_2 = (t_2 + 2p_+'^0 k_1'^0)/(2p_+'^0 k_1'^0)$ and $p_+'^0 = (s_{1345} - t_1)/(2\sqrt{s_{1345}})$,

$$k_4''^{\mu} = \frac{\lambda^{1/2}(s_{345}, s_{35}, 0)}{2\sqrt{s_{345}}}(1, -\cos\phi_3 \sin\theta_3, -\sin\phi_3 \sin\theta_3, -\cos\theta_3), \tag{A.9}$$

and

$$\begin{aligned} k_3'''^{\mu} &= \frac{\sqrt{s_{35}}}{2}(1, \cos\phi_4 \sin\theta_4, \sin\phi_4 \sin\theta_4, \cos\theta_4), \\ k_5'''^{\mu} &= (k_3'''^0, -\vec{k}_3'''). \end{aligned} \tag{A.10}$$

The four-momenta k_1, k_3, k_4, and k_5 in the CM system are obtained from the four-momenta k_1', k_3''', k_4'', and k_5''' by applying the appropriate Lorentz transformations, as for instance described in Ref. [30].

Acknowledgement

We thank D. Graudenz and R. Pittau for useful discussions about Monte Carlo integration and T. Stelzer for discussions concerning Madgraph.

References

[1] G. Bélanger and F. Boudjema, *Phys. Lett.* **B288** (1992) 201;
G. Abu Leil and W.J. Stirling, *J. Phys.* **G21** (1995) 517;
W.J. Stirling and A. Werthenbach, DTP-99-30, hep-ph/9903315.

[2] V. Barger, T. Han and R.J.N. Phillips, *Phys. Rev.* **D39** (1989) 146;
W. Beenakker, K. Kołodziej and T. Sack, *Phys. Lett.* **B258** (1991) 469;
W. Beenakker, F.A. Berends and T. Sack, *Nucl. Phys.* **B367** (1991) 287;
K. Kołodziej and M. Zrałek, *Phys. Rev.* **D43** (1991) 3619;
J. Fleischer, F. Jegerlehner and K. Kołodziej, *Phys. Rev.* **D47** (1993) 830;
H. Tanaka, T. Kaneko and Y. Shimizu, *Comput. Phys. Commun.* **64** (1991) 149;
E.N. Argyres, O. Korakianitis, C.G. Papadopoulos and W.J. Stirling, *Phys. Lett.* **B259** (1991) 195.

[3] R.G. Stuart, Phys. Lett. **B262** (1991) 113;
H. Veltman, *Z. Phys.* **C62** (1994) 35;
A. Aeppli, F. Cuypers and G.J. van Oldenborgh, *Phys. Lett.* **B314** (1993) 413.

[4] A. Aeppli, G.J. van Oldenborgh and D. Wyler, *Nucl. Phys.* **B428** (1994) 126.

[5] W. Beenakker and A. Denner, *Int. J. Mod. Phys.* **A9** (1994) 4837;
W. Beenakker et al., in *Physics at LEP2*, eds. G. Altarelli, T. Sjöstrand and F. Zwirner (CERN 96-01, Geneva, 1996), Vol. 1, p. 79, hep-ph/9602351.

[6] M. Böhm et al., *Nucl. Phys.* **B304** (1988) 463;
J. Fleischer, F. Jegerlehner and M. Zrałek, *Z. Phys.* **C42** (1989) 409.

[7] D.Yu. Bardin, S. Riemann and T. Riemann, *Z. Phys.* **C32** (1986) 121;
F. Jegerlehner, *Z. Phys.* **C32** (1986) 425;
A. Denner and T. Sack, *Z. Phys.* **C46** (1990) 653.

[8] W. Beenakker, A.P. Chapovsky and F.A. Berends, *Phys. Lett.* **B411** (1997) 203 and *Nucl. Phys.* **B508** (1997) 17;
A. Denner, S. Dittmaier and M. Roth, *Nucl. Phys.* **B519** (1998) 39 and *Phys. Lett.* **B429** (1998) 145.

[9] W. Beenakker, A.P. Chapovsky and F.A. Berends, DTP-98-90, hep-ph/9811481.

[10] A. Aeppli and D. Wyler, *Phys. Lett.* **B262** (1991) 125.

[11] A. Aeppli, doctoral thesis, Universität Zürich (1992).

[12] G.J. van Oldenborgh, P.J. Franzini and A. Borrelli, *Comput. Phys. Commun.* **83** (1994) 14.

[13] G.J. van Oldenborgh, *Nucl. Phys.* **B470** (1996) 71.

[14] J. Fujimoto et al., *Nucl. Phys. (Proc. Suppl.)* **37B** (1994) 169.

[15] F. Caravaglios and M. Moretti, *Z. Phys.* **C74** (1997) 291.

[16] F.A. Berends, R. Pittau and R. Kleiss, *Nucl. Phys.* **B424** (1994) 308.

[17] K. Fujikawa, *Phys. Rev.* **D7** (1973) 393;
M. Bacé and N.D. Hari Dass, *Ann. Phys.* **94** (1975) 349;
B.W. Lee and R.E. Shrock, *Phys. Rev.* **D16** (1977) 1444;
M.B. Gavela, G. Girardi, C. Malleville and P. Sorba, *Nucl. Phys.* **B193** (1981) 257;
N.G. Deshpande and M. Nazerimonfared, *Nucl. Phys.* **B213** (1983) 390;
F. Boudjema, *Phys. Lett.* **B187** (1987) 362;
A. Denner, S. Dittmaier and R. Schuster, *Nucl. Phys.* **B452** (1995) 80.

[18] S. Dittmaier, *Phys. Rev.* **D59** (1999) 016007.

[19] F.A. Berends, P.H. Daverveldt and R. Kleiss, *Nucl. Phys.* **B253** (1985) 441 and *Comput. Phys. Commun.* **40** (1986) 285;
J. Hilgart, R. Kleiss and F. Le Diberder, *Comput. Phys. Commun.* **75** (1993) 191.

[20] R. Kleiss and R. Pittau, *Comput. Phys. Commun.* **83** (1994) 141.

[21] M. Böhm, W. Hollik and H. Spiesberger, *Fortschr. Phys.* **34** (1986) 687;
A. Denner, *Fortschr. Phys.* **41** (1993) 307;
A. Denner, S. Dittmaier and G. Weiglein, *Nucl. Phys.* **B440** (1995) 95.

[22] D. Bardin et al., *Nucl. Phys. (Proc. Suppl.)* **37B** (1994) 148.

[23] D. Bardin et al, in *Physics at LEP2*, eds. G. Altarelli, T. Sjöstrand, F. Zwirner, CERN 96-01, Vol. 2, p. 3, hep-ph/9709270.

[24] E. Boos and Th. Ohl, Darmstadt preprint IKDA-99-06, hep-ph/9903357.

[25] T. Stelzer and W.F. Long, *Comput. Phys. Commun.* **81** (1994) 357;
E. Murayama, I. Watanabe and K. Hagiwara, KEK report 91-11, 1992.

[26] W. Beenakker et al., *Nucl. Phys.* **B500** (1997) 255.

[27] G. López Castro, J.L.M. Lucio and J. Pestieau, *Modern Physics Letters* **A40** (1991) 3679.

[28] R.G. Stuart, in Z^0 *Physics*, ed. J. Tran Thanh Van (Editions Frontieres, Gif-sur-Yvette, 1990) p. 41.

[29] U. Baur and D. Zeppenfeld, *Phys. Rev. Lett.* **75** (1995) 1002;
C.G. Papadopoulos, *Phys. Lett.* **B352** (1995) 144;
E.N. Argyres et al., *Phys. Lett.* **B358** (1995) 339.

[30] E. Byckling and K. Kajantie, Particle Kinematics, John Wiley & Sons, London (1973), p. 158ff.

[31] F. Boudjema et al, in *Physics at LEP2*, eds. G. Altarelli, T. Sjöstrand, F. Zwirner, CERN 96-01, Vol. 1, p. 207, hep-ph/9601224.